

eISSN 2657-7291

2020 (LXI)
Vol. 222, No. 3

SCIENTIFIC JOURNAL OF POLISH NAVAL ACADEMY

Formerly ZESZYTY NAUKOWE AKADEMII MARYNARKI WOJENNEJ



Gdynia 2020

SCIENTIFIC BOARD

Rear Adm. Tomasz Szubrycht, Prof. (Chairman), Polish Naval Academy, Poland
Rear Adm. Vergil Chitac, Prof. PhD, Naval Academy, 'Mircea cel Batran', Romania
Franciszek Grabski, Prof., Polish Naval Academy, Poland
Capt (N) Kalin Kalinov, Prof. PhD, Nikola Vaptsarov Naval Academy, Bulgaria
Gvidonas Labeckas, Prof., Aleksandras Stulginskis University, Litwa
Commodore Boyan Mednikarov, Prof. DSc, Nikola Vaptsarov Naval, Bulgaria
Jerzy Merkisz, Prof., Poznan University of Technology, Poland
Suleyman Ozkaynak, Prof., Piri Reis University, Turkey
Rear Adm. Juan L. Sobrino Pérez-Crespo, Spain
Takeshi Shinoda, Prof., Kyushu University, Japan

EDITORIAL COMMITTEE

Editor-in-Chief
Zygmunt Kitowski, Prof.

Managing Editor, Executive Editor
Beata Róžańska, MSc

Associate Editors
Andrzej Grządziela, Ass. Prof. (*Mechanical Engineering*)
Jerzy Garus, Ass. Prof. (*Automatic Control, Electronics
and Electrical Engineering*)

Language Editor
James Marson, MSc, Eng.
Agata Antoniuk, MSc

Andrzej Felski, Prof. (*Civil Engineering and Transportation*)
Ryszard Studański, PhD Eng. (*Technical Computer Sciences
and Telecommunications*)

Statistical Editor
Agata Załęska-Fornal, PhD Eng.

All articles in the quarterly have been peer reviewed

The original (reference) version of the journal is the online version

Abstracting & Indexing

Arianta
Baidu Scholar
BazTech
CEON Biblioteka Nauki
CNKI Scholar (China National Knowledge
Infrastructure)
CNPIEC
Dimensions
DOAJ
EBSCO Discovery Service
Google Scholar

Index Copernicus
J-Gate
KESLI-NDSL (Korean National Discovery for Science Leaders)
Naviga (Softweco)
POL-index
Primo Central (ExLibris)
ReadCube
Summon (Serials Solutions/ProQuest)
TDNet
WorldCat (OCLC)

Website quarterly

<https://content.sciendo.com/view/journals/sjpna/sjpna-overview.xml>

<https://www.amw.gdynia.pl/index.php/nauka/czasopisma-naukowe/item/45-zeszyty-naukowe>

Journal Owner and Publisher

Akademia Marynarki Wojennej/Polish Naval Academy

Contact

Redakcja Zeszytów Naukowych AMW

Akademia Marynarki Wojennej

Inż. J. Śmidowicza 69, 81-127 Gdynia

tel. 261 26 29 72

e-mail: b.rozanska@amw.gdynia.pl; wydawnictwo@amw.gdynia.pl

CONTENTS

Bogdan Żak and Stanisław Hożyń

Controlling the Operation of a Ship's Electric Power Supply Using Fuzzy Controllers 1

Waldemar Mironiuk, Arkadiusz Panasiuk, and Marek Szymoński

The Effect on Constant Heel on Circulation of a Vessel Calculated on the Basis
of Investigations of M/S "Ziemia Zamojska" Model 14

Franciszek Grabski

Nonhomogeneous Generalisations of Poisson Process in the Modeling of Random
Processes Related to Road Accidents 29

Vadim Romanuke

Pilot Symbol Error Re - Orthogonalization in 2×2 MIMO Systems of Wireless
Communication..... 43

Czesław Dyrz

Ice Drift in the Arctic Ocean 68



CONTROLLING THE OPERATION OF A SHIP'S ELECTRIC POWER SUPPLY USING FUZZY CONTROLLERS

Bogdan Żak¹ , **Stanisław Hożyń²** 

Polish Naval Academy, Faculty of Mechanical and Electrical Engineering, Śmidowicza 60 Str., 81-127 Gdynia, Poland, e-mail: ¹b.zak@amw.gdynia.pl, ²s.hozyn@amw.gdynia.pl, ORCID ID: ¹0000-0002-6640-7116, ²0000-0003-1422-0330.

ABSTRACT

The paper presents dynamical models of controlling voltage and frequency of ship's electric supply set. The simulation model of synchronous generator, implemented in Matlab/Simulink, was described. For the developed simulation model, developed control systems using fuzzy controllers type P and PD were presented. Simulation research for resistance, inductive and capacitive loads were carried out for these regulators. Sample results of simulation tests are presented in the form of voltage waveforms at the output of the generator and rotational speed of the internal combustion engine for various load conditions. The conducted tests allow to assess the quality of the control process using fuzzy controllers and thus ensure the selection of the optimal solution.

Keywords:

Control, fuzzy controller, electric power supply

Research article

© 2020 Bogdan Żak, Stanisław Hożyń

This journal provides immediate open access to its content under the Creative Commons by 4.0 license.

Authors who publish with this journal retain all copyrights and agree to the terms of the above-mentioned [CC BY 4.0 license](https://creativecommons.org/licenses/by/4.0/)

INTRODUCTION

Modern power systems of vessels are designed to ensure the continuity of generation and supply of electricity to consumers and to ensure the quality of supplied energy. To meet the requirements, each ship's power supply system is equipped with automatic control systems, in which there are two regulators, one task is to regulate the voltage generated by the generator, while the other regulates the frequency. The main tasks of the control system of synchronous generator voltage is to maintain constant voltage at its terminals. Since most generators used in ships is self-excited synchronous generators wherein the coil winding is powered by its own rectified voltage generator. This solution means that excitation voltage is not constant, but decreases with increasing load. The main tasks of the control system of synchronous generator frequency is to maintain a constant frequency in both the states of static and dynamic. This is directly connected to the maintenance of constant rotational speed of generator's driving motor [6], [7]. It follows that a major problem in the design of this type of system is the issue of the selection of controls systems which fulfill the requirements given to the generated electricity on ships [3]. In current solutions, these are classic controllers based on the numerical representation of input and output signals. Alternative to this approach can be fuzzy logic control systems. In fuzzy control systems, signals are represented by linguistic variables. Thanks to this, a set of rules in the form of conditional sentences is used to control the object [10]. Seemingly a departure from the sharp representation of the variable values of the regulation process in favor of a fuzzy and unclear linguistic interpretation seems to be pointless. However, observations of the surrounding world force to draw different conclusions. As evidence, one can give the behavior of a man whose action in everyday life is based on blurred premises, and yet it turns out to be effective [1],[5]. Given the above premises, the authors developed fuzzy controllers for controlling the ship's electric power supply and conducted their simulation tests. The presented work shows the results of simulation tests.

SIMULATION MODEL OF SHIP'S ELECTRIC POWER SUPPLY SET

Developing a model of the system, or the phenomenon, involves clarifying the fundamental mathematical relationships between certain physical phenomena.

At the same time it missed many details and features of real object irrelevant from the point of view of the modeling.

To consider, a mathematical model of the synchronous machine has adopted the following simplification [2, 4, 9]:

- assumed symmetry of three-phase windings of the stator and rotor,
- it is assumed that the magnetomotive force in the gap along the pole pitch has sinusoidal distribution,
- neglected hysteresis, saturation, anisotropy and eddy currents in the magnetic circuit,
- it is assumed that the operating point of the magnetic circuit is located in the linear part of the characteristics of the magnetization, which in practice means accepting fixed self-inductance values as well as cross-inductance,
- the generator is carried out without attenuating windings with the rotor pole pieces made from solid steel.

Taking into account the assumptions the equation describing the dynamics of the synchronous generator can be represented as follow [2], [4]:

$$u_{sd} = \frac{dF_{sd}}{dt} - NF_{sq} + R_s i_{sd} \quad (1)$$

$$u_{sq} = \frac{dF_{sq}}{dt} - NF_{sd} + R_s i_{sq} \quad (2)$$

$$\frac{dF_f}{dt} = -\frac{1,5R_f M_{wd}}{L_{sd}L_f - 1,5M_{wd}^2} F_{sd} - \frac{R_f L_{sd}}{L_{sd}L_f - 1,5M_{wd}^2} F_f + u_f \quad (3)$$

$$F_{sq} = L_{sq} i_{sq} \quad (4)$$

$$F_{sd} = \left(i_{sd} + \frac{M_{wd} F_f}{L_{sd}L_f - 1,5M_{wd}^2} \right) \left(\frac{L_{sd}L_f - 1,5M_{wd}^2}{L_f} \right) \quad (5)$$

$$M_e = p(F_{sd} i_{sq} - F_{sq} i_{sd}) \quad (6)$$

where:

M_e – electromagnetic moment,

N – the speed of rotation of the magnetic field,

u_f, i_f –voltage and excitation current brought to the side of the stator,

F_f – the magnetic flux associated with the winding excitation, brought to the site of the stator,

p – the number of pole pairs,

R_f, L_f – resistance and self-inductance of winding excitation, brought to the site of the stator,

L_{sd}, L_{sq} – self-inductance of the stator windings in the longitudinal, and transverse axis,

M_{wd} – mutual inductance between the excitation winding, and the replacement of the stator winding in the longitudinal axis,

R_s – stator resistance,

F_{sd}, F_{sq} – space vector of the stator magnetic flux in the longitudinal and transverse axes,

i_{sd}, i_{sq} – stator current in the longitudinal and transverse axes.

Complementary to the previous system of equations is equation of moments written in the following form:

$$n = \frac{1}{J} \int_0^t (M_m - M_e) dt - T_r n \quad (7)$$

where:

M_m – mechanical torque applied from the outside, produced by the combustion engine,

J – the moment of inertia of the rotating mass,

n – the angular speed of rotation of the rotor,

T_r – coefficient of friction.

These equations correspond to the ideal synchronous machine with the adoption of the classic simplifying assumptions. On their basis, in MATLAB / Simulink, a simulation model of electric power supply set installed on ships type Oliver Hazard was developed. Its block diagram is shown in Fig.1. The simulation model developed allows changing the generator parameters using a dialog box. In addition, this model can simulate different impedance values loading the generator using the model's "z" and "cs" inputs.

Verification studies of the simulation model of synchronous generator were carried out using the presented model. Verification was made by measuring the characteristics of idling and regulatory, and compare them with the real condition characteristics [6, 8]. The simulation model developed allows changing the generator parameters using a dialog box. However, using the "z" and "cs" inputs of the model, one can simulate different types and values of load. Using the "z" input, enter the value of the load resistance, while through the "cs" input, phase shift resulting from the type of load. The test results are shown in Fig.2.

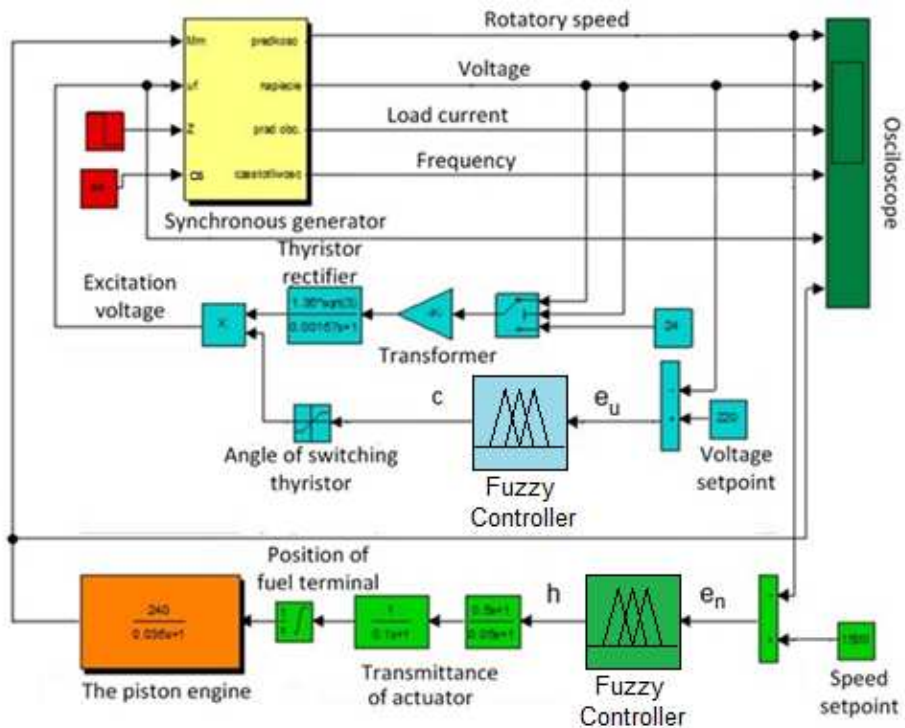


Fig. 1. Model of control system of electric power supply set

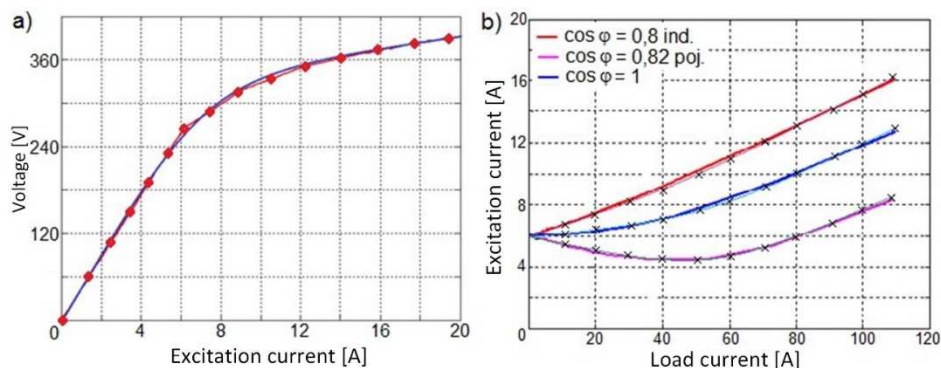


Fig. 2. The characteristics of the real generator and the simulation model: a) idle (blue color – the real generator; red dots – model), b) regulatory (continuous line – the real generator, crosses – model)

FUZZY CONTROLLER

The use of fuzzy logic occurs in simple loops, usually controlled by PID controllers. The use of fuzzy logic makes it possible to mimic the operation of a PID controller with modifications that allow obtaining nonlinear control [9] [10]. Intuitively, it seems that the use of a PID controller is the most advantageous solution. However, the amount of work involved in developing an extensive rule base, as well as the time-consuming heuristic matching of the scaling gain factors, lead to doubts as to whether the hypothetical improvement of the adjustment rates compensates for the designer's efforts.

For this reason, the work analyzes the control system with a fuzzy controllers type P and type PD to determine the suitability of each of them in the control system of a ship's electric power supply. The purpose of the developed regulators is to stabilize the rotational speed of the combustion engine driving the generator, and the excitation voltage of the synchronous generator, so as to ensure that the rated voltage and frequency of the generated voltage are maintained when the load changes [1], [7].

The synthesis started with the pre-selection of membership function of each controller, and to write the rules database [10]. The initial simulation verification was carried out, consisting in determining the correctness of assumptions for the structures of controllers prepared in such a way. Intuitive changes were made

in the shapes and arrangement of membership functions, and the rule bases were corrected. As a result of the analyzes carried out, P-type controller and PD-type controller were developed for both controlled quantities, for which the functions of belonging to sets of fuzzy controller inputs have the form as in Fig. 3 and Fig. 4

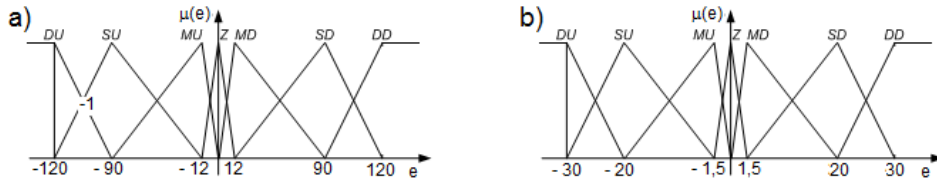


Fig. 3. The functions belonging to fuzzy sets for the regulator type P: a) speed controller, b) voltage controller.

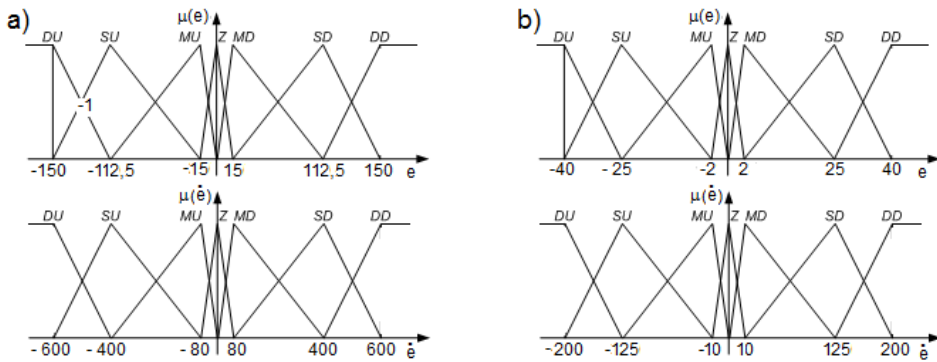


Fig. 4. The functions belonging to fuzzy sets for the regulator type PD: a) speed controller, b) voltage controller.

The interference was made on the basis of the created base of rules, whose inference principles were conducted in accordance with Table 1 for the P-type controller, and Table 2 for the PD-regulator. Interference was made on the basis of established database of rules, where the rules of conclusion were conducted according with table 1 for the P type controller, and table 2 for the PD type controller. In the tables were determined: DU – a big negative, SU – medium negative, MU – small negative, Z - zero, DD – big positive, SD – medium positive, MD – small positive. Rules in database were defined on the basis of expert knowledge.

Table 1. Database of rules for P type controller

e	DU	SU	MU	Z	MD	SD	DD
u	DD	SD	MD	Z	MD	SU	DU

Table 1. Database of rules for PD type controller

	e							
		DU	SU	MU	Z	MD	SD	DD
de/dt	DU	DD	DD	SD	SD	SU	SU	DU
	SU	DD	SD	MD	MD	MU	MU	SU
	MU	SD	MD	MD	Z	Z	Z	MU
	Z	DD	SD	MD	Z	MU	SU	DU
	MD	MD	Z	Z	Z	MU	MU	SU
	SD	SD	MD	MD	MU	MU	SU	DU
	DD	DD	SD	SD	SU	SU	DU	DU

Defuzzification of resulting membership function of conclusions rule base was carried out by the method of center of gravity according to the membership function shown in Fig.5.

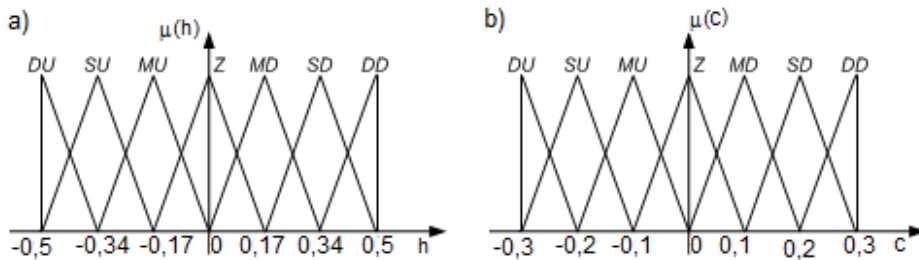


Fig. 5. Fuzzy sets used in the process of defuzzification: a) for speed controller, b) for voltage controller

SIMULATION RESEARCHES

For the developed model of the control system of the ship's electric power supply, tests of the voltage and rotational speed control system were carried out with the use of P and PD fuzzy controllers. The tests were carried out for a step change in the load of the synchronous generator from 0 to 60%, and from 50% to 100% of the rated power of various types of load. The course of the fuel rail position and excitation voltage at the step change of load was also examined. Examples of the results of the simulation are shown in the Fig. 6 to Fig.10. During the simulation tests were also carried out a comparative study of classical and fuzzy controllers. An example of the results of comparative tests is shown in Figure 11.

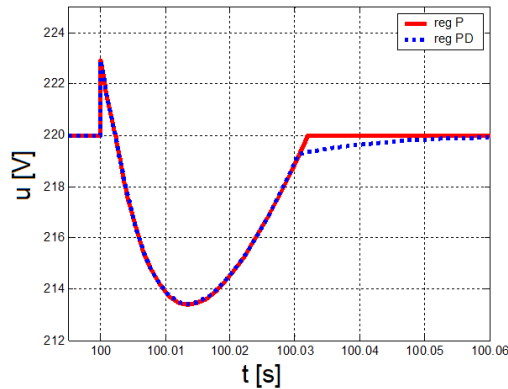


Fig. 6. Course of the generator's voltage during step change of load from 0 to 60% of rated power for fuzzy controllers P and PD for resistive load.

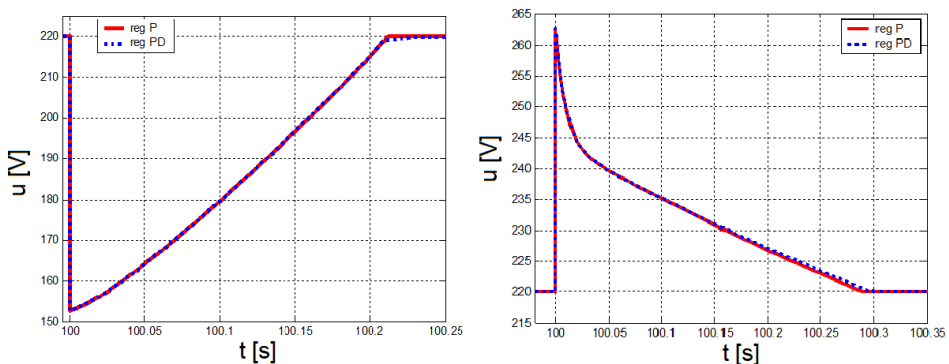


Fig. 7. Course of the generator's voltage during step change of load from 0 to 60% of rated power for fuzzy controllers P and PD: a) inductive load $\cos(\varphi) = 0,4$; b) the capacitive load $\cos(\varphi) = 0.8$.

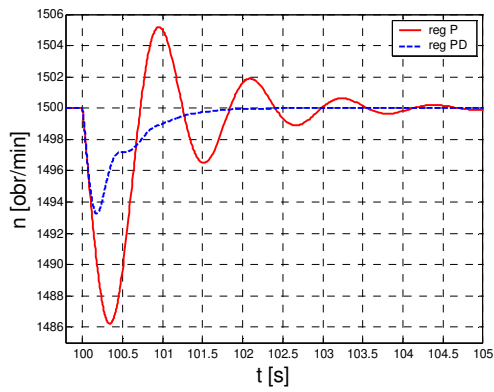


Fig. 8. The course of rotational speed during step change of load from 0 to 60% of rated power for fuzzy controllers P and PD for resistive load.

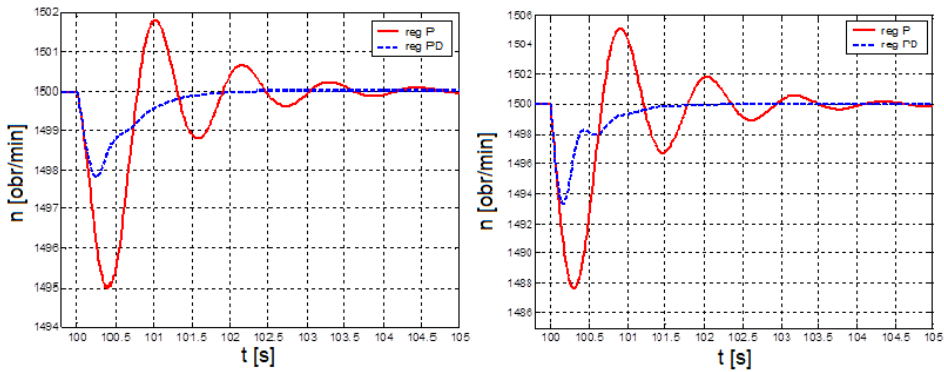


Fig. 9. The course of rotational speed during step change of load from 0 to 60% of rated power for fuzzy controllers P and PD: a) for inductive load, $\cos(\phi) = 0.4$; b) for capacitive load $\cos(\phi) = 0.8$.

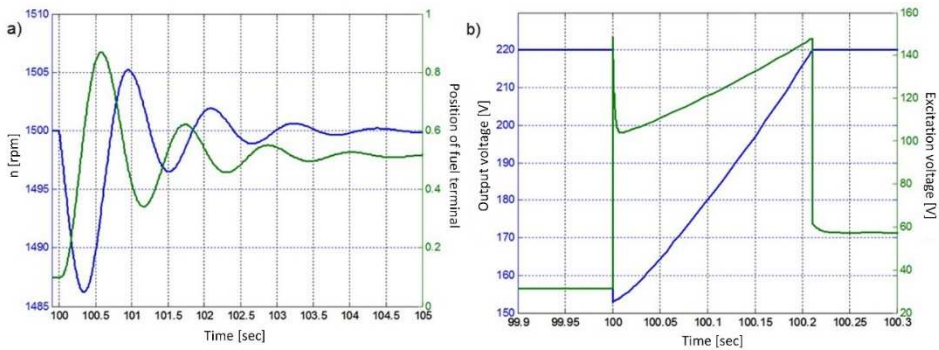


Fig. 10. The course during step change of load for fuzzy controller P: a) the speed and position of the fuel terminal, b) the value of the output voltage and the excitation voltage

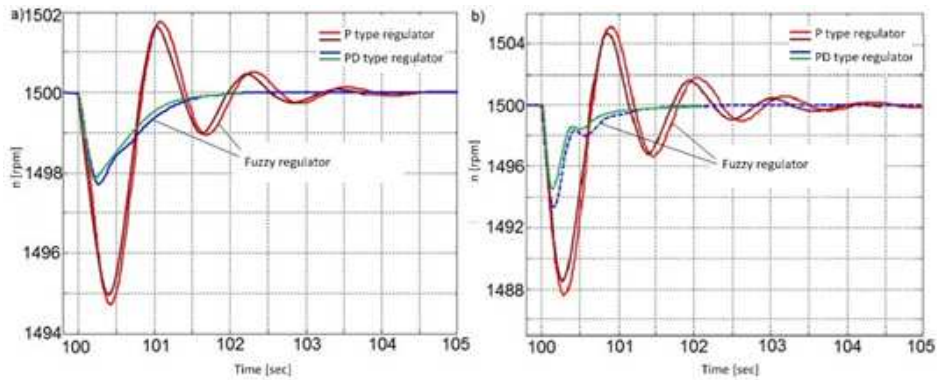


Fig. 5. The course of rotational speed during step change of load from 0 to 60% of rated power for controllers P and PD classic and fuzzy: a) for inductive load, b) for capacitive load.

CONCLUSIONS

When assessing the duration of the transition process, the advantage of the controller type PD over the controller type P is clearly visible, with fuzzy controllers ensuring good control quality in both cases. Assuming the permissible deviation from the speed setpoint ± 1 rpm, the time of practical determination of the rotational speed course at a step change in load from 0 to 60% of the rated power at a resistive load was 2.3 [s] for the controller type P, while for the controller type PD 1 [s]. For capacitive and inductive loads, these times were slightly different. For this system, the steady-state error has been reduced to zero.

Referring the obtained test results to the guidelines of Qualification Societies regarding the change of the rotational speed of the drive motor of the electric power supply when the load changes, it should be stated that the proposed solutions of fuzzy controllers fully fulfill the tasks set before it.

In the present system there was reported maximum voltage drop to 70% of the nominal voltage. Such value of squat voltage does not depend on the controller of voltage, but on the electromagnetic generator. For its value the greatest impact has rather subtransient reactance, which depends on the leakage reactance of the stator winding. A small value of the subtransient reactance results in a lower voltage drop on terminals of the generator. For this reason, examined voltage fuzzy controllers type P and PD gives the same voltage waveforms during step change in load.

The maximum voltage increase, the error in the steady state, and the duration of the transient process of applying, both classic and fuzzy controllers, are within the limits set by the Society for Qualifying.

Comparing the obtained waveforms of output signals for a step change in load, it should be stated that both classic and fuzzy controllers ensure the correct course of transition processes. These processes for both types of P and PD controllers classic and fuzzy are very similar, therefore from the point of view of control quality classic controllers can be replaced by fuzzy controllers.

The further direction of research on the use of fuzzy regulators to stabilize the electrical parameters of the ship's power supply set will be focused on the development of fuzzy PID controllers.

REFERENCES

- [1] Brzozka J., "Regulators and automation systems" [in Polish], Micom, Warsaw 2004.
- [2] Grunwald Z., "Electric drive" [in Polish], WNT, Warsaw 1987.
- [3] Kowalski Z., Tittenbrun S., Łatkowski W., "Adjusting the rotational speed of marine diesel engines" [in Polish], Marine Publisher, Gdańsk 1988.
- [4] Latek W., "The theory of electrical machines" [in Polish], WNT, Warszawa 1982.
- [5] Piegat, A., "Modeling and fuzzy control, Warsaw", Akademicka Publishing House EXIT, 2003.
- [6] Technical documentation of Diesel Generator Set Model 114J000 With GTRB Starting Air Compressor.
- [7] Wyszowski S., "Marine Electrical Engineering" [in Polish], Marine Publisher, Gdańsk 1991.
- [8] Zhang X. M., Long S. Y., "Simulation study of fuzzy PID controller for DC motor based on DSP", 2012 International Conference on Industrial Control and Electronics Engineering, 978-0-7695-4792-3/13, 2012 IEEE, DOI 10.1109/ICICEE.2012.430.
- [9] Żak B., Hożyń S., "Dynamic models of control voltage and frequency for electric power supply set" [in Polish], Science notebooks PNA, year XLVIII, no 169 K/1 2007, pp. 199-206.
- [10] Żak A., Żak B., "Selected issues of the control of marine objects" [in Polish], Ship Automation, L&L, Gdańsk 2010.

STEROWANIE PRACĄ OKRĘTOWEGO ZESPOŁU ZASILANIA ELEKTRYCZNEGO ZA POMOCĄ RE- GULATORÓW ROZMYTYCH

STRESZCZENIE

W pracy przedstawiono dynamiczne modele sterowania napięciem i częstotliwością zestawu zasilającego statku. Opisano model symulacyjny generatora synchronicznego, zaimplementowany w Matlab / Simulink. Dla opracowanego modelu symulacyjnego przedstawiono rozwinięte układy sterowania wykorzystujące sterowniki rozmyte typu P i PD. Dla tych regulatorów przeprowadzono badania symulacyjne dla obciążeń rezystancyjnych, indukcyjnych i pojemnościowych. Przykładowe wyniki testów symulacyjnych przedstawione są w postaci przebiegów napięcia na wyjściu generatora i prędkości obrotowej silnika spalinowego dla różnych warunków obciążenia. Przeprowadzone testy pozwalają ocenić jakość procesu sterowania za pomocą rozmytych regulatorów, a tym samym zapewnić wybór optymalnego ich rozwiązania.

Słowa kluczowe:

Stabilizacja, sterowanie rozmyte, zasilanie elektryczne



THE EFFECT ON CONSTANT HEEL ON CIRCULATION OF A VESSEL CALCULATED ON THE BASIS OF INVESTIGATIONS OF M/S “ZIEMIA ZAMOJSKA” MODEL

Waldemar Mironiuk¹ Arkadiusz Panasiuk²
Marek Szymoński³

Polish Naval Academy, Faculty of Navigation and Naval Weapons, Śmidowicza 69 Str., 81-127 Gdynia, Poland, e-mail: w.mironiuk@amw.gdynia.pl, a.panasiuk@amw.gdynia.pl, m.szymonski@amw.gdynia.pl, ORCID ID: ¹0000-0001-7931-3680, ²0000-0003-1873-9025, ³0000-0002-7234-7623

ABSTRACT

The article presents modeling research on the M/S "Ziemia Zamojska" reduced model, carried out in an open fresh water area by a team of employees of the Department of Operating of Floating Vessels, Polish Naval Academy, Gdynia. The research involved circulating the model with constant angle of heel on the selected side, and the main engine set to full speed ahead. Using a real ship to carry this type of investigations is risky. It may lead to some failures like e.g. rudder failure, steering gear malfunction, overload and in some circumstances even main engine seizure. For this reason, ships are not tested with the rudder put to starboard or to port at the full speed ahead setting, even during a "Crash Stop" maneuver. However, based on the analysis of accidents at sea, and practical experience, it appears that during real operating conditions of vessels, there may occur situations when, for the sake of safety, the maneuver mentioned above must be carried out. Therefore, the authors had to conduct model tests of a floating vessel for the described case of ship operation

Keywords:

Ship maneuvering, tests of maneuvering properties, reduction model

Research article

© 2020 Waldemar Mironiuk, Arkadiusz Panasiuk, Marek Szymoński

This journal provides immediate open access to its content under the Creative Commons by 4.0 license.

Authors who publish with this journal retain all copyrights and agree to the terms of the above-mentioned [CC BY 4.0 license](#)

INTRODUCTION

Design of ships or marine structures requires a series of specialist analyzes and simulations. The purpose of these activities is to make sure the planned facilities comply with the assumed operational characteristics, and safe performance standards in changing weather conditions at sea [2,6].

Scientific modelling research is not only the basic and universal method used to forecast the dynamic properties of a ship, especially at the design stage, but also has a great significance in scientific and research, both as a method of theory verification, and as an autonomous cognitive method [3,6]. The idea of modelling research assumes making inferences concerning the performance of a real object based on the measurements carried out on a model. The results of such tests are used, among others, for forecasting nautical and maneuvering properties of ships, and other floating objects[1,7].

This article describes modeling research on the M/S "Ziemia Zamojska" reduced model, carried out in an open fresh water area by a team of employees of the Department of Operating of Floating Vessels, Polish Naval Academy, Gdynia. The basic particulars of the ship are as follows:

$L_{pp} = 172 \text{ m}$

$B = 23 \text{ m}$

$T = 9.85 \text{ m}$

$H = 13.90 \text{ m}$

Weight of empty ship: 6 622 T

DWT = 26 706 T

Freeboard : 4.086 m

The main object used in the research was a reduced model of the bulk carrier M/S "Ziemia Zamojska", whose construction was based on the theoretical lines on 1:75 scale [9,11]. The model was studied under non-typical operating conditions. The investigations involved circulating the model with constant angle of heel, and the main engine set to full speed ahead [8,10]. To conduct such investigations only models of floating vessels can be used. Using a real ship to carry this type of investigations is risky as some failures may occur, e.g. rudder failure, steering gear malfunction, overload, and, in some circumstances, even main engine seizure. For this reason, ships are not tested with the rudder put to starboard, or to port at the full

speed ahead setting, even during a "Crash Stop" maneuver. However, under real operating conditions of vessels, there may occur situations when, for the sake of safety, the maneuver mentioned above must be carried out. Therefore, the authors had to conduct investigations using a floating vessel and check the performance of the model for the described case of ship operation.

MANEUVERING TESTS OF MODEL OF M/S "ZIEMIA ZAMOJSKA"

Maneuvering tests of the model of bulk carrier M/S "Ziemia Zamojska" were carried out in freshwater. This required the preparation of measuring equipment, selecting the site and testing methodology. To this end, the model of the vessel was balanced in the laboratory conditions, and proper operation of the sensors used to measure the angle of heel, draft, and propulsion system was verified. To record the positioning of the unit Leica Viva receiver and controller were used, and then the data obtained was processed with the Leica Geo Office software [5]. Changes in the heel of the reduced model in the course of circulation were recorded with a Simex angle of heel meter. During the investigations, the possibilities of using the built-in tilt sensors, and the apparatus recording the model's motion parameters, were also checked. In the experiment the impact of the initial heel of the model on the size and shape of the circulation diameter was investigated. Owing to the use of appropriate measuring devices the necessary information were collected and documented.

DESCRIPTION OF PLACE USED TO CARRY OUT INVESTIGATION OF MODELS

The circulation investigations of the model of "Ziemia Zamojska" with heel were carried out on a freshwater pond in Kosakowo. The total area of the basin is 2550 [m²], and its average depth is 4 [m].

The research in the basin was carried out in the following weather conditions: NNW wind approx. 0.5-1.0 [m / s], temperature 23 [° C], moderate cloud cover. To measure temperature, wind direction, and speed one used a mobile meteorological station, which offered the capability of monitoring of test conditions.

Figure 1 presents a photo of the water body in which maneuvering investigations of the model were carried out. To fix the position of the model on the water, and to facilitate the calculation of the position coordinates one made a range light

using Leica Viva GS15 receiver, and Leica Viva CS15 controller. It is marked in the Figure below with numbers 1 and 2. The position fixing accuracy of the range light is 0.004 [m]. The circulations of the model were marked with colors: red to the right, and blue to the left.



Fig. 1 A satellite photo of the maneuvering area together with the mapped maneuvering range and traces of circulation [14]

MEASURING INSTRUMENTS

The instruments for measuring the angle of heel and draft of the model were fitted in the hull. Immersion sensors were fitted in the bow and stern area of the model. The places where the immersion sensors were fitted are shown in Fig. 2.



Fig. 2 An arrangement of sensors used to measure draft of ship's model [11]

The results of measurements recorded with the measuring sensors during the circulation of the model of M/S "Ziemia Zamojska" are sent via a remote transmission system, and read out at the CMC shore station. The system's operating range should not exceed 750 m. During the tests, the distance between the model and the recording station was 10 to 40 m, it was within the range of the data transmission system. The selected water area was free of interference from other devices operated in the test area.

The shore station of the measuring system includes the Simex Multicon CMC recorder, radio modem with antenna, gel batteries supplying the station, power supply unit, converter. The 1.5 GB internal memory of the recorder allowed storage of the measurement data. Fig. 3 shows a photo of the shore station.



Fig 3. MultiCon CMC [11]

In order to monitor the current position of the model during circulation, the DGPS RTK system, and mobile devices suitable for the size of the test object, i.e. a 120-channel Leica Viva GS15 receiver, were used. It can receive both GLONASS and GPS signals, and record data having frequency of up to 20 [Hz]. According to the manufacturer's data, the positioning accuracy of the model is as follows:

horizontal: 10 [mm]

vertical: 20 [mm].

A photo of Leica Viva GS15 is shown in Fig.4.



Fig. 4 Leica Viva GS15 [13]

The coordinates of the tracked vessel can be fixed when appropriate algorithms are used in the internal software. The receiver allows tracking satellites over the horizon, working with reference station networks, and quick initialization in the RTK mode. The device can communicate with the controller thanks to the Bluetooth connection installed. [5]

The Leica Viva CS15 controller, shown in Fig. 5, is a modern, powerful portable computer which allows to save the parameters of the observations carried out.



Fig. 5 Leica Viva CS15 Controller [13]

During the preparation for the investigations, both of the above devices were fitted in the holds of the ship's model. The Leica Viva GS15 receiver was fitted in the hold of model No. 4, and the Leica Viva CS15 controller in the hold of the model No. 2. To ensure the model was "on an even keel" position, additional weights were placed in hold 1. Fig. 6 shows a photograph of the ship's model during the maneuvering tests with GPS devices placed inside.



Fig. 6 Ship's model during circulation investigations [4,11]

The photo above shows the investigated ship's model during circulation to starboard. A number of tests were performed during the investigations, and the averaged results are presented in the next chapter.

THE RESULTS OF RESEARCH ON CIRCULATION OF SHIP'S MODEL

The model-based research on circulation was carried out with a constant initial heel to port and starboard. Before starting the tests, it was necessary to take measures to balance the reduced model of the ship, and bring it to a "on an even keel" position. In addition, in order to obtain a permanent heel to port or starboard $\varphi=3.5^\circ$, the ship's model had to be properly ballasted.

The investigations were carried out for circulation to the starboard, and port side. The number of RPM in the main engine was set for Full Speed Ahead, and the rudder deflection was 35° on each side ("to port" and "to starboard").

The results of circulation are shown in Figures 7 and 8, and in Table 1, and Table 2, respectively.

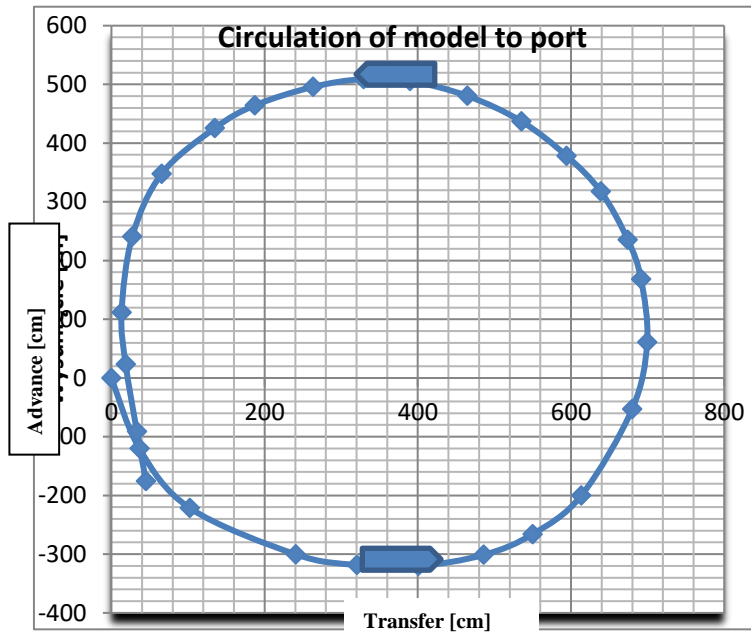


Fig. 7 The results of circulation of the model with heel to port [4]

Table 1. Parameters of circulation presented in Fig. 7

Object	Setting	Loading condition	Initial ship speed [kn]	Rudder angle [°]	Diameter [m]	Frontal shift [m]	End time [s]
Tilted model	FSA	Fully loaded	1.4	35	8.2	6.06	26

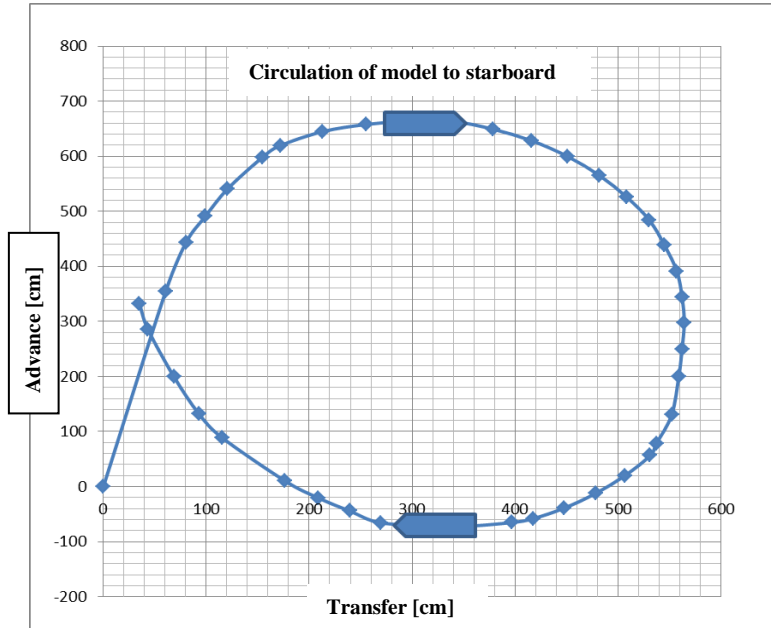


Fig. 8 The results of circulation of the model with heel to starboard [4]

Table 2. Parameters of circulation presented in Fig. 8

Object	Setting	Loading condition	Initial ship speed [kn]	Rudder angle [°]	Diameter [m]	Frontal shift [m]	End time [s]
Model with heel	FSA	Fully loaded	1.4	35	7.4	7.06	20

COMPARISON OF THE RESULTS OF CIRCULATION OF THE MODEL WITH INITIAL HEEL, AND WITH NO HEEL

In the next stage of the research, the results of circulation of M/S "Ziemia Zamojska" model were compared, in the same loading condition, loaded with ballast and GPS devices, with no initial heel, and with constant heel to port $\varphi = 3.5^\circ$.

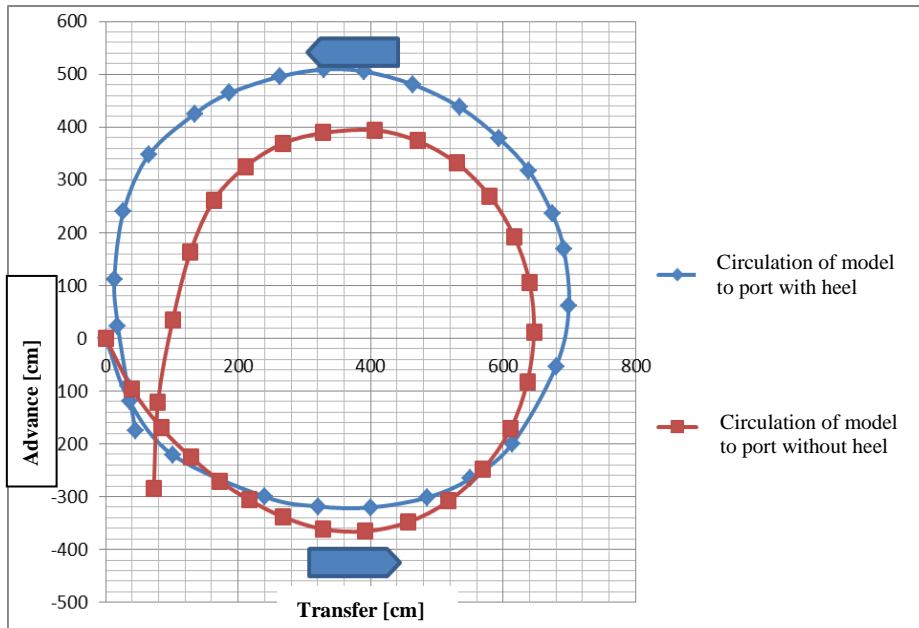


Fig. 9 The results of circulation of the model to port with heel and with no heel [4]

Table 3. Circulation parameters from Fig. 9 used for comparison

Object	Setting	Loading condition	Initial ship speed [kn]	Rudder angle [°]	Diameter [m]	Frontal shift [m]	End time [s]
Model with heel	FSA	Full loading	1.4	35	8.2	6.06	26
Model with no heel	FSA	Full loading	1.4	35	7.4	3.7	59

The circulation of the M / S "Ziemia Zamojska" model to starboard was compared in a similar way. The model was in the same loading condition and was loaded

with ballast and GPS devices. The investigations were carried out for the model with no constant initial heel, and with constant heel to port equal to $\varphi = 3.5^\circ$.

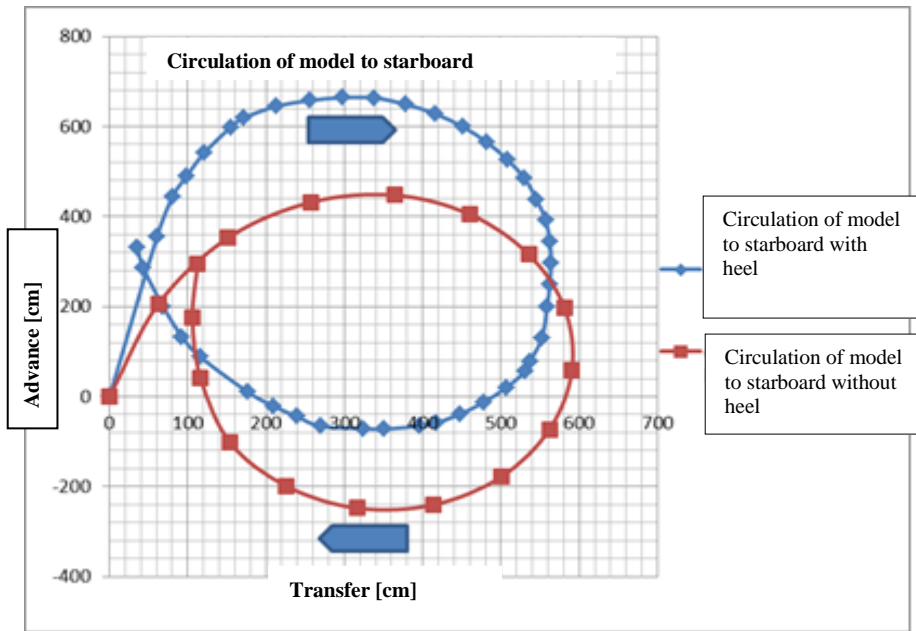


Fig. 10 Comparison of circulation to starboard with no heel and with heel [4]

Table 4. Comparative parameters of circulation with no heel and with heel.

Object	Setting	Loading condition	Initial ship speed [kn]	Rudder angle [°]	Diameter [m]	Frontal shift [m]	End time [s]
Model with heel	FSA	Full loading	1.4	35	7.4	7.06	20
Model with no heel	FSA	Full loading	1.4	35	7.0	4.5	30

During the research, it was noticed that the reduced model of bulk carrier M/S "Ziemia Zamojska" was slightly trimmed by the bow when moving forward, despite the fact that it was with no trim before the start of the research. The forced

constant heel to starboard caused the necessity to correct the course of the tested model using the rudder.

The introduction of a fixed initial angle of heel to port of 3.5° caused the average circulation of the reduced model to increase slightly by 0.8 [m] during circulation to port, and 0.4 [m] during circulation starboard. The cause of this phenomenon was the asymmetrical shape of the immersed part of the hull of the investigated model, and the excessive speed of the model during circulation which disrupted the distribution of the behind propeller flow and its impact on the rudder blade. In addition, the model uses a right-hand propeller generating the tendency to change course to starboard.

During the circulation investigations, the angle of heel of the reduced model was also recorded. The operating centrifugal force, and propeller lateral force had a significant impact on its magnitude. When the model circulated to port it righted due to the centrifugal force action, and the initial constant heel was reduced to zero. However, during a right-hand maneuver, the initial angle of heel 3.5° increased to 10° . During this investigation, the angle of heel increased after covering about a quarter of the distance.

CONCLUSIONS

Summing up the obtained results of the investigations, it can be stated that the angle of heel of the model causes predicted changes in the parameters measured during the circulation maneuver. The main goal of the research was to demonstrate the impact of the initial angle of heel of the investigated model on the magnitude of the circulation radius and angle of heel.

It follows from the analysis of the results of circulation of the model, with and with no heel, that the constant, initial angle of heel of the vessel increases the diameter of circulation during maneuvers both to the starboard and port.

In the case of circulation to port, the introduced constant angle of heel of the model contributed to the reduced angle of heel to zero, and thus to righting the vessel. However, in the case of the right-handed circulation maneuver, a significant increase in the angle of heel of the model up to 10° was recorded. In addition, during this maneuver, the investigated reduced model produced ellipse wake pattern, whereas during the action to maneuver to port the wake had a circle-like pattern.

The duration of the maneuver with no heel was similar to the duration of the maneuver with heel. A slight blowing of wind did not affect the investigations.

The data obtained in the research will be significant for the planning and implementation of the next stage of research in which maneuvering of the M/S "Ziemia Zamojska" model will be assisted by tug models.

REFERENCES

- [1.] Duda D., *Manewrowanie statkiem o napędzie mechanicznym.*, Wyższa Szkoła Morska, Gdynia 1973
- [2.] Gucma M. *Models of maritime safety for development of navigation support systems.* The Archives of Transport 2016, Volume 37, Issue 1.
- [3.] Jacyna M.; Wasiaś M.; Lewczuk K.; Kłodawski M. *Simulation model of transport system of Poland as a tool for developing sustainable transport.* Archives of Transport 2014, No 3, Volume 31.
- [4.] Jarzyna N., *Wpływ przechyłu na cyrkulację jednostki na przykładzie modelu statku m/s "Ziemia Zamojska" praca dyplomowa*, AMW Gdynia 2017
- [5.] Mikołajczyk M., *Odbiorniki i kontrolery Leica Viva, Nawi.* Dodatek GNSS geodety. Marzec 2011, nr 1, s. 14 - 16.
- [6.] Mironiuk W. *Model-based investigations on dynamic ship heels in relation to maritime transport safety.* The Archives of Transport 2015, Volume 33, Issue 1.
- [7.] Nowicki A., *Wiedza o manewrowaniu statkami morskimi*, Trademar, Gdynia 1999
- [8.] Sobieszczański T., *Manewrowanie statkiem morskim*, Tom I, Skrypt niekomercyjny, AMW Gdynia 2014
- [9.] Sztolpa M., *Próby manewrowe modelu m/s „Ziemia Zamojska” na wybranym akwencie śródkowodnym oraz ocena ich podobieństwa do wyników prób jednostki rzeczywistej*, Praca dyplomowa, Gdynia 2016
- [10.] Wróbel F., *Vademecum nawigatora*, Trademar, Gdynia 2013
- [11.] Materiały dot. modelu statku „Ziemia Zamojska” KEJP AMW Gdynia
- [12.] <http://surveyequipment.com/>
- [13.] <http://www.geoland-surveying.com/>
- [14.] <http://maps.google.com/>

WPŁYW STAŁEGO KĄTA PRZECHYŁU NA CYRKULACJĘ STATKU, OKREŚLONY NA PODSTAWIE BADAŃ MODELU M/S „ZIEMIA ZAMOJSKA”

STRESZCZENIE

W artykule przedstawiono opis badań modelowych modelu redukcyjnego statku M/S „Ziemia Zamojska”, przeprowadzonych na akwenu otwartym z wodą słodką przez zespół pracowników Katedry Eksploatacji Jednostki Pływającej AMW w Gdyni. Badania te polegały na wykonaniu cyrkulacji modelu statku ze stałym kątem przechyłu na wybraną burtę, utrzymując nastawę pracy silnika głównego w pozycji cała naprzód (CN). Przeprowadzenie takich testów na rzeczywistym statku jest ryzykowne. Może to doprowadzić do awarii np. steru, maszyny sterowej, przeciążenia, a nawet w szczególnych okolicznościach zatarcia silnika głównego. Z tego powodu na statkach nie prowadzi się testów polegających na wychyleniu steru na burtę przy nastawie CN, nawet podczas manewru „Crash Stop”. Na podstawie analizy wypadków na morzu, oraz z doświadczeń praktycznych, wynika, że podczas rzeczywistej eksploatacji jednostek pływających zdarzają się sytuacje, w których w celu zachowania bezpieczeństwa należy wykonać wymieniony manewr. Wymusiło to na autorach przeprowadzenia badań modelowych jednostki pływającej w opisanym przypadku eksploatacyjnym.

Słowa kluczowe:

Manewrowanie statkiem, badania właściwości manewrowych, model redukcyjny, cyrkulacja



DOI: 10.2478/sjpna-2020-0009



NONHOMOGENEOUS GENERALISATIONS OF POISSON PROCESS IN THE MODELING OF RANDOM PROCESSES RELATED TO ROAD ACCIDENTS

Franciszek Grabski 

Polish Naval Academy, Department of Mathematics and Physics, Śmidowicza 69 Str., 81-127 Gdynia, Poland, e-mail: f.grabski@amw.gdynia.pl, ORCID ID: 0000-0001-5772-4550

ABSTRACT

The stochastic processes theory provides concepts, and theorems, which allow to build the probabilistic models concerning accidents. "Counting process" can be applied for modelling the number of road, sea, and railway accidents in the given time intervals. A crucial role in construction of the models plays a Poisson process and its generalizations. The nonhomogeneous Poisson process, and the corresponding nonhomogeneous compound Poisson process are applied for modelling the road accidents number, and number of people injured and killed in Polish roads. To estimate model parameters were used data coming from the annual reports of the Polish police.

Keywords:

road accident, nonhomogeneous Poisson process, nonhomogeneous compound Poisson process

Research article

© 2020, Franciszek Grabski

This journal provides immediate open access to its content under the Creative Commons by 4.0 license. Authors who publish with this journal retain all copyrights and agree to the terms of the above-mentioned [CC BY 4.0 license](https://creativecommons.org/licenses/by/4.0/)

1. INTRODUCTION

Von Bortkiewitsch (1898) calculated, using the data of the Prussian army, the number of soldiers who died, during 20 consecutive years, because of being kicked by a horse. He noticed that a random variable, say X , denoting the number of solders killed accidentally by the horse kick per year, has approximately Poisson distribution with parameter $\lambda=0.61$ [1/year]. Since then Poisson's distribution, and the corresponding stochastic Poisson process, have found use in various fields of science and technology.

A Poisson process and its extensions, are used in safety and reliability problems. They allow to construct the models denoting number of road, sea, and railway accidents in the given time intervals.

It should be mentioned, that this paper is an extension of article [3], because of the new data concerning the Polish road accidents in 2019 [11].

2. NONHOMOGENEOUS POISSON PROCESS

We start from definition of nonhomogeneous Poisson Process (NPP).

Let

$$\tau_0 = \vartheta_0 = 0, \quad \tau_n = \vartheta_1 + \vartheta_2 + \dots + \vartheta_n, \quad n \in \mathbb{N}, \quad (1)$$

where $\vartheta_1, \vartheta_2, \dots, \vartheta_n$ are positive independent random variables.

$$\tau_\infty = \lim_{n \rightarrow \infty} \tau_n = \sup\{\tau_n: n \in \mathbb{N}_0\}. \quad (2)$$

A stochastic process $\{N(t): t \geq 0\}$ defined by the formula

$$N(t) = \sup\{n \in \mathbb{N}_0: \tau_n \leq t\} \quad (3)$$

is called a *counting process* corresponding to a random sequence $\{\tau_n: \in \mathbb{N}_0\}$.

Let $\{N(t): t \geq 0\}$ be a stochastic process, taking values on $S = \{0,1,2, \dots\}$, value of which represents the number of events in a time interval $[0, t]$.

A counting process $\{N(t): t \geq 0\}$ is said to be *nonhomogeneous Poisson process* (NPP) with an intensity function $\lambda(t) \geq 0, t \geq 0$, if

1. $P(N(0) = 0) = 1$; (4)

2. The process $\{N(t): t \geq 0\}$ is the stochastic process with independent increments, the right continuous and piecewise constant trajectories;

3. $P(N(t+h) - N(t) = k) = \frac{(\int_t^{t+h} \lambda(x) dx)^k}{k!} e^{-\int_t^{t+h} \lambda(x) dx}$; (5)

From the definition it follows, that the one dimensional distribution of NPP is given by the rule:

$$P(N(t) = k) = \frac{(\int_0^t \lambda(x) dx)^k}{k!} e^{-\int_0^t \lambda(x) dx}, \quad k = 0, 1, 2, \dots \quad (6)$$

The expectation and variance of NPP are the functions:

$$\Lambda(t) = E[N(t)] = \int_0^t \lambda(x) dx \qquad V(t) = V[N(t)] = \int_0^t \lambda(x) dx, \quad t \geq 0. \quad (7)$$

The corresponding standard deviation is:

$$D(t) = \sqrt{V[N(t)]} = \sqrt{\int_0^t \lambda(x) dx}, \quad t \geq 0. \quad (8)$$

The expected value of the increment $N(t+h) - N(t)$ is:

$$\Delta(t; h) = E(N(t+h) - N(t)) = \int_t^{t+h} \lambda(x) dx. \quad (9)$$

The corresponding standard deviation is :

$$D(t; h) = D(N(t+h) - N(t)) = \sqrt{\int_t^{t+h} \lambda(x) dx} \quad (10)$$

A nonhomogeneous Poisson process with $\lambda(t) = \lambda, t \geq 0$ for each $t \geq 0$, is a regular Poisson process. The increments of nonhomogeneous Poisson process are independent, but not necessarily stationary. A nonhomogeneous Poisson process is a Markov process.

3. NONHOMOGENEOUS COMPOUND POISSON PROCESS

We assume that $\{N(t): t \geq 0\}$ is a *nonhomogeneous Poisson process* (NPP) with an intensity function $\lambda(t)$, $t \geq 0$ such that $\lambda(t) \geq 0$ for $t \geq 0$, and X_1, X_2, \dots is a sequence of the independent random variables independent of $\{N(t): t \geq 0\}$. A stochastic process

$$X(t) = X_1 + X_2 + \dots + X_{N(t)}, \quad t \geq 0 \quad (11)$$

is said to be a *nonhomogeneous compound Poisson process* (NCP).

Proposition 1.

Let $\{X(t): t \geq 0\}$ be a *nonhomogeneous compound Poisson process* (NCP).

If $E(X_1^2) < \infty$, then:

$$1. \quad E[X(t)] = \Lambda(t) E(X_1) \quad (13)$$

$$2. \quad V[X(t)] = \Lambda(t) E(X_1^2), \quad (14)$$

Where:

$$\Lambda(t) = E[N(t)] = \int_0^t \lambda(x) dx.$$

P r o o f [6].

Corollary 1

Let $\{X(t+h) - X(t): t \geq 0\}$ be an increment of a *nonhomogeneous compound Poisson process* (NCP).

If $E(X_1^2) < \infty$, then:

$$E[X(t+h) - X(t)] = \Delta(t; h) E(X_1), \quad (15)$$

$$V[X(t+h) - X(t)] = \Delta(t; h) E(X_1^2), \quad (16)$$

where:

$$\Delta(t; h) = \int_t^{t+h} \lambda(x) dx. \quad (17)$$

4. DATA ON MOTORIZATION AND ROAD ACCIDENTS IN POLAND

Quoted data from the Central Statistical Office from 2017, 2018, and 2019 were presented in reports of the Polish Police [9], [10], [11].

4.1 GENERAL DATA ON MOTORIZATION

Since the beginning of the 90's, the number of vehicles registered in Poland has been systematically growing

Tab.1. Number of motor vehicles in the years 2007-2018

Years	Motor vehicles in total	Passenger cars	Trucks	Motorcycles
2007	19 471 836	14 588 739	2 345 068	825 305
2008	21 336 913	16 079 533	2 511 677	909 144
2009	22 024 697	16 494 650	2 595 845	974 906
2010	23 037 149	17 239 800	2 767 035	1 013 014
2011	24 189 370	18 125 490	2 892 064	1 069 195
2012	24 875 718	18 744 412	2 920 779	1 107 260
2013	25 683 575	19 389 446	2 962 064	1 153 169
2014	26 472 274	20 003 863	3 037 427	1 189 527
2015	27 409 106	20 723 423	3 098 376	1 272 333
2016	28 601 037	21 675 388	3 179 655	1 355 625

2017	29 149 178	22 109 572	3 212690	1 398 609
2018	29 656 238	22 514 047	3 249 961	1 428 299
2019	31 388 643	23 874 531	3 387 536	1 553 370

It is easy to count, that from 2007 to 2019, the number of passenger cars increased by 38.68 %, number of trucks by 30.77%, while the number of motorcycles increased by 46.68% . During this time, the total number of motor vehicles increased by 37.96%.

The location of our country on the East-West transport route generates heavy transit traffic. According to the border guards, cited in the police report [10], in 2018, 12 435 345 vehicles entered the European Union's external borders, including 9 970 787 passenger cars.

4.2 GENERAL DATA ON ROAD ACCIDENTS

A table, containing the number of accidents, and their consequences, is presented below. The data comes from police reports [9], [10]. [11].

Tab.2. Number of accidents and their consequences in the years 2007-2019

Years	Interval [days]	Center of interval	Number of accident	Number of fatalities	Number of injured	Indica- tor α	Indicator β
2007	[0, 365)	183,5	49 536	5 583	63 224	0,1127	1,2763
2008	[365, 731)	548	49 054	5 432	62 097	0,1108	1,2658
2009	[1096,1461)	1278,5	44 196	4 572	56 046	0,1034	1,2681

2010	[1461,1826)	1643,5	38 832	3 907	48 952	0,1006	1,2606
2011	[1826,2192)	2008,5	40 065	4 189	49 501	0,1045	1,2355
2012	[2192,2558)	2375	37 046	3 571	45 792	0,0963	1,236
2013	[2558, 2923)	2740,5	35 847	3 357	44 059	0,0957	1,2571
2014	[2923, 3288)	3105,5	34 970	3 209	42 545	0,0915	1,2166
2015	[3288, 3653)	3470,5	32 967	2 938	39 778	0,0891	1,2066
2016	[3653, 4019)	3836	33 664	3 026	40 766	0,0898	1,2109
2017	[4019, 4384)	4201,5	32 760	2 831	39 466	0,0864	1,2047
2018	[4384, 4749)	4566,5	31 674	2 862	37 359	0,0903	1,1794
2019	[4749, 5114)	4931,5	30 288	2 909	35 477	0,0960	1,1713

The table does not contain the number of traffic collisions. For example, in 2018, 436 414 road collisions were reported.

5. MODEL OF THE ROAD ACCIDENT NUMBERS

Due to the nature of these events, pre-assumption that it is a nonhomogeneous Poisson process with some parameter $\lambda(t) > 0$, seems to be justified. The expected value of increment of this process is given by (9), while its one dimensional distribution is determined by (5). We can use practically these rules if the intensity

function $\lambda(t) > 0$ is known. To define this function one utilizes information presented in table 2. The statistical analysis of the data shows that the intensity function $\lambda(t)$ can be approximated by the linear function $\lambda(t) = at + b$.

5.1. ESTIMATION OF THE MODELS PARAMETERS

Dividing the number of accidents in each year, by 365 or 366 we get the intensity in units of [1 / day].

We approximate the empirical intensity by a linear regression function $y = ax + b$ that satisfies condition

$$S(a, b) = \sum_{i=1}^n [y_i - (ax_i + b)]^2 \rightarrow \min$$

Recall, that solution of above optimization problem leads to finding parameters a and b . The parameters are given by the rules:

$$a = \frac{\mu_{11}}{\mu_{20}}, \quad b = m_{01} - am_{10}, \quad \bar{x} = m_{10} = \frac{1}{n} \sum_{i=1}^n x_i, \quad \bar{y} = m_{01} = \frac{1}{n} \sum_{i=1}^n y_i, \quad (22)$$

$$m_{11} = \frac{1}{n} \sum_{i=1}^n x_i y_i, \quad \mu_{11} = m_{11} - m_{10} m_{01},$$

$$m_{20} = \frac{1}{n} \sum_{i=1}^n x_i^2, \quad \mu_{20} = m_{20} - m_{10}^2.$$

Applying the rules (26) for the data from Table 2 and using Excel system we obtain:

$$a = -0.000003658, \quad b = 2,534128 \quad (23)$$

The linear intensity of accidents is:

$$\lambda(x) = -0,000113629 x + 3.442384 \geq 0 \quad (24)$$

This function is shown in figure 1.

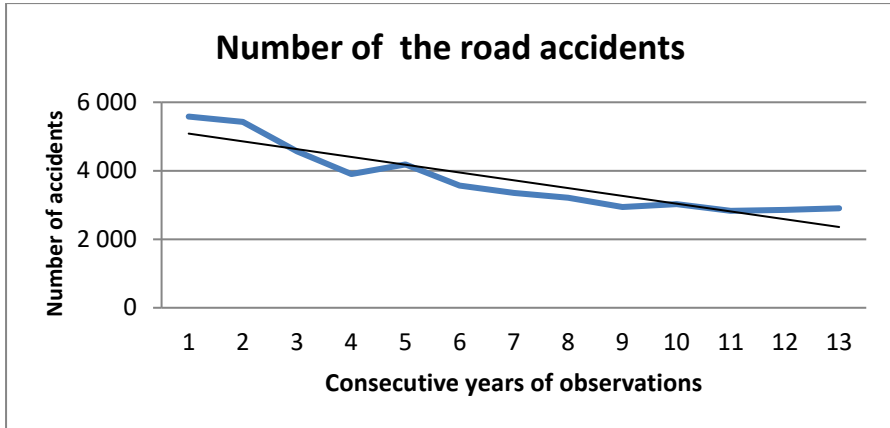


Fig. 1. Intensity of the road accidents in Poland

From (7) we obtain:

$$\Lambda(t) = -0,000113629 t^2 + 2,534128t, \quad t \geq 0. \tag{25}$$

Therefore the one dimensional distribution of NPP is:

$$P(N(t) = k) = \frac{(\Lambda(t))^k}{k!} e^{-\Lambda(t)} \quad k = 0,1,2, \dots, \tag{26}$$

where $\Lambda(t)$ is given by (25).

Finally one can say that the model of the accident number on Polish roads is the nonhomogeneous Poisson process with the parameter $\Lambda(t)$, $t \geq 0$, determined by (25).

Using data from the Table 1 and Figure 2 one can compute the indicator of fatalities intensity in road accidents in relation to the number of vehicle crossing

$$\alpha = \mathbf{NF} / \mathbf{NVC} \tag{27}$$

where \mathbf{NF} denotes number of fatalities, \mathbf{NVC} designates number of vehicles crossing

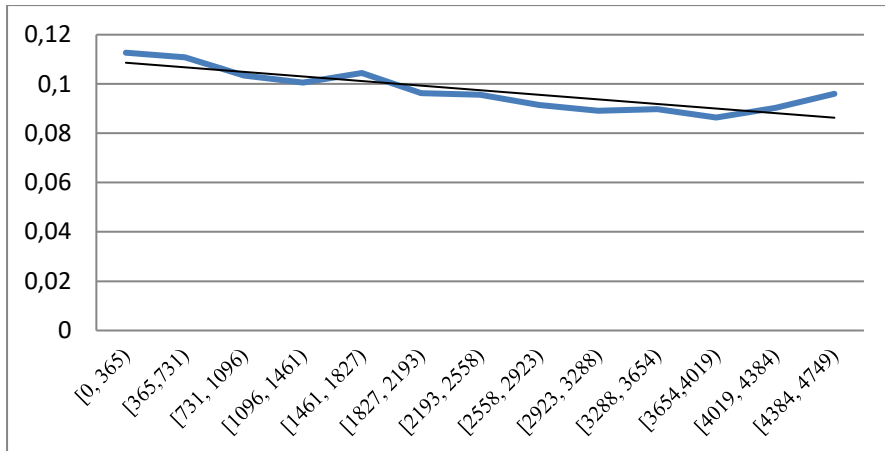


Fig. 2. Indicators of fatalities intensity in road accidents in relation to the crossing number

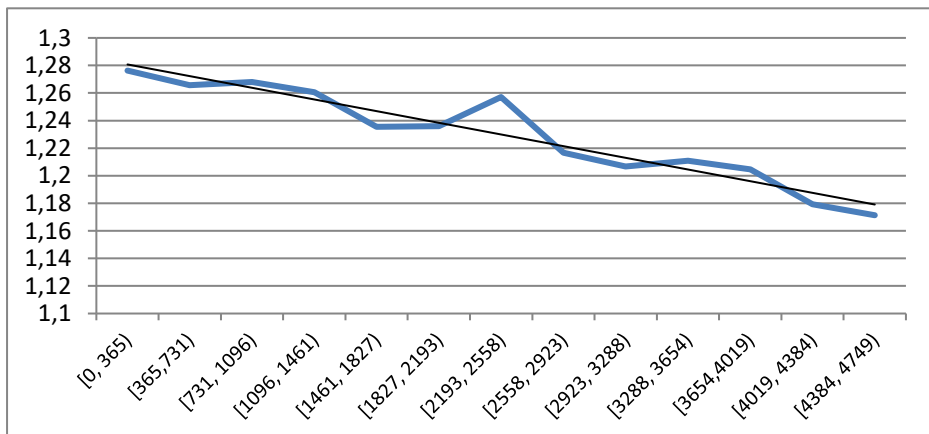


Fig. 3. Indicators of injured intensity in road accidents in relation to the crossing number

$$\beta = NI/NVC$$

6. ANTICIPATION OF ACCIDENT NUMBER

From (5) and (10) we get:

$$P(N(t+h) - N(t) = k) = \frac{\Delta(t;h)}{k!} e^{-[\Delta(t;h)]}. \quad (28)$$

It means that one can anticipate number of accidents at any time interval, with a length of h . The expected value of the increment $N(t+h) - N(t)$ is defined by (10). For the function:

$$\Lambda(t) = a \frac{t^2}{2} + b t \quad (29)$$

we obtain the expected value of the accidents at time interval $[t, t+h)$

$$\Delta(t; h) = h \left(\frac{a h}{2} + b + a t \right), \quad (30)$$

The corresponding standard deviation is:

$$\sigma(t; h) = \sqrt{h \left(\frac{a h}{2} + b + a t \right)}. \quad (31)$$

Example 1.

We want to predict the number of accidents from June 1st of 2020 to August 30th of 2020. We also want to calculate the probability of a given number of accidents. First we have parameters t and h . As extension of table 2 on year 2019 we can obtain an interval [4749, 5114]. From January 1st of 2020 to June 1st of 2020 152 days have passed. Hence $t = 4749 + 152 = 4901$. From June 1st to August 31st $h = 92$ days have passed. For these parameters using (29) and (30) we obtain $\Delta(t; h) = 7074.406$, $\sigma(t; h) = 84.109$.

This means, that the average predicted number of accidents between June 1st, 2019 and August 31st, 2019 is about 7074, with a standard deviation of about 84.

$$P_{c \leq X \leq d} = P(c \leq N(t+h) - N(t) \leq d) = \sum_{x=c}^{x=d} \frac{7074.406^x}{x!} e^{-7074.406}; x = 0, 1, 2, \dots$$

Applying approximation by normal distribution we get:

$$P_{c \leq X \leq d} = \Phi \left(\frac{d - 7074,406}{84,109} \right) - \Phi \left(\frac{c - 7074,406}{84,109} \right)$$

For $d = k\sigma$, $c = -k\sigma$, $k = 1, 2, 3$ we obtain k -sigma formula:

$$P_{-k\sigma \leq X \leq k\sigma} = 2\Phi(k) - 1 = \begin{cases} 0.6827 & \text{for } k = 1 \\ 0.9545 & \text{for } k = 2 \\ 0.9973 & \text{for } k = 3 \end{cases}$$

Therefore, for the predicted number of accidents between June 1st, 2019 and August 31st, 2019:

$$\begin{aligned} P(X \in [6990.297, 7158.515]) &= 0.6827, \\ P(X \in [6906.188, 7242.624]) &= 0.9545, \\ P(X \in [6822.079, 7326.733]) &= 0.9973. \end{aligned}$$

6.1. ANTICIPATION OF THE ACCIDENTS CONSEQUENCES

Let $X = X_i$, $i = 1, 2, \dots, N(t)$ denotes number of fatal events in a single accident. We suppose that the random variables X_i , $i = 1, 2, \dots$ have the identical Poisson distribution with parameters $E(X_i) = V(X_i) = \mu$, $i = 1, 2, \dots, N(t)$.

The predicted number of fatal events in the time interval $[t, t + h)$ is described by the expectation of the increment $X(t + h) - X(t)$. Recall that the expected value, and standard deviation of the accidents number in the time interval $[t, t + h)$ are given by (10) and (11). For the data from *Example 1* using (29) and (30), we obtain the expected value of fatalities number (**EFN**), and the corresponding standard deviation (**DFN**) in the time interval $[t, t + h) = [4900, 4992)$:

$\Delta(t; h) = \Delta(t; h) \times \mu$, and $\mathbf{DFN} = \sqrt{\Delta(t; h) \times (\mu + \mu^2)}$. We assume that the NCPP is homogenous in this time interval, and a mean is calculated in center of interval.

Finally we obtain **EFN = 315.034** and **DFN = 17.7492**.

For the same data we obtain the expected value of injured number, denoted by **EIN**, and corresponding standard deviation (**DIN**) in the time interval $[4900, 4992)$. We assume that the NCPP is homogenous in this time interval, and a mean is calculated in center of that one. In this case $\Delta(t; h) = 626.62$. Using the same formulas we get the expectation **EIN**, and the standard deviation **DGN = 25,03** of injured people number.

7. CONCLUSIONS

The nonhomogeneous Poisson process, and the corresponding nonhomogeneous compound Poisson process are applied for modelling the road accidents number, and the number of injured and fatalities on Polish roads. To estimate model parameters one used data coming from the annual reports of the Polish police. Constructed models allowed to anticipate number of accidents at any time interval, with a length of h and the accident consequences. One obtained the expected value of fatalities or injured, and the corresponding standard deviation in the time interval $[t, t + h)$.

The statistical distribution of fatalities number in a single accident, and statistical distribution of injured people number, and also statistical distribution of fatalities or injured number in a single accident, are computed.

REFERENCES

- [1] Di Crescenzo A., Martinucci B., Zacks S. Compound Poisson process with Poisson subordinator *Journal of Applied Probability* Vol. 52, No. 2, p. 360- 374, 2015.
- [2] Fisz M. Probability and Mathematical Statistics, Warsaw PWN; (in Polish) 1969
- [3] Grabski F. Nonhomogeneous Poisson process and compound Poisson process in modeling of random processes related to road accidents. *Journal of KONES Powertrain and Transport*, Vol.26, No.1 2019. Pp 39-46.
- [4] Grabski F. *Semi-Markov Processes: Applications in Systems Reliability and Maintenance* Elsevier; Amsterdam, Boston, Heidelberg, London, NewYork, Oxford, Paris, San Diego, San Francisco, Sydney, 2015.
- [5] Grabski F. Nonhomogeneous Poisson process application to modelling accidents numberat Baltic waters and ports. *Journal of Polish Safety and Reliability Association*; volume 8, number 1, p. 39-46, 2017.
- [6] Grabski F. Nonhomogeneous stochastic processes connected to Poisson process. *Scientific Journal of Polish Naval Academy*, 2 (213), pp. 5-15, Gdynia 2018 (LIX).
- [7] Limnios N, Oprisan G., *Semi-Markow Processes and Reliability*; Birkhauser, Boston 2001.
- [8] Shiriyayev A. N., *Probability*. Springer-Verlag, New York, Berlin, Heidelberg, Tokyo 1984.
- [9] Symon E. *Wypadki drogowe w Polsce w roku 2017* . Wydział Opiniodawczo-Analityczny Biura Ruchu Drogowego Komendy Głównej Policji, Warszawa 2018.

[10] Symon E. *Wypadki drogowe w Polsce w roku 2018*. Wydział Opiniotawczo-Analityczny Biura Ruchu Drogowego Komendy Głównej Policji, Warszawa 2019.

[11] Symon E. *Wypadki drogowe w Polsce w roku 2019*. Wydział Opiniotawczo-Analityczny Biura Ruchu Drogowego Komendy Głównej Policji, Warszawa 2020.

NIEJEDNORODNE UOGÓLNIENIE PROCESU POISSONA W MODELOWANIU LOSOWYCH PROCESÓW ZWIĄZANYCH Z WYPADKAMI DROGOWYMI

STRESZCZENIE

W pracy przedstawiono niektóre uogólnienia procesu Poissona i ich własności. Skupiono się na dwóch uogólnieniach – niejednorodnym procesie Poissona i niejednorodnym złożonym procesie Poissona. Niejednorodny proces Poissona pozwala na skonstruowanie modelu probabilistycznego, opisującego liczbę różnych rodzajów wypadków. Niejednorodny złożony proces Poissona pozwala matematycznie opisywać konsekwencje tych wypadków. Przedstawione tu wyniki teoretyczne dają możliwość przewidywania liczby wypadków i ich konsekwencji. Estymacja parametrów modelu została wykonana na podstawie danych zamieszczonych w rocznych raportach Policji [9], [10], [11].

Słowa kluczowe:

wypadek drogowy, niejednorodny proces Poissona, niejednorodny złożony proces Poissona



PILOT SYMBOL ERROR RE-ORTHOGONALIZATION IN 2×2 MIMO SYSTEMS OF WIRELESS COMMUNICATION

Vadim Romanuke 

Polish Naval Academy, Faculty of Mechanical and Electrical Engineering, Śmidowicza 69 Str., 81-127 Gdynia, Poland; e-mail: v.romanuke@amw.gdynia.pl; ORCID ID: 0000-0003-3543-3087

ABSTRACT

A 2×2 MIMO wireless communication system with channel estimation is simulated, in which two transmit, and two receive antennas are employed. The orthogonal pilot signal approach is used for the channel estimation, where the Hadamard sequences are used for piloting. Data are modulated by coherent binary phase-shift keying, whereupon an orthogonal space-time block coding subsystem encodes information symbols by using the Alamouti code. Based on the simulation, it is ascertained a possibility to decrease the bit-error rate by substituting the Hadamard sequences for the sequences having irregular structures, and constituting the eight known orthogonal bases. Considering a de-orthogonalization caused by two any pilot sequence symbol errors, the bit-error rate is decreased by almost 2.9 %. If de-orthogonalizations are caused by two repeated indefinite, and definite pilot sequence symbol errors, the decrements are almost 16 % and 10 %, respectively. Whichever sequences are used for piloting, the 2×2 MIMO system is ascertained to be resistant to the de-orthogonalization if the frame is of 128 to 256 symbols piloted with 32 to 64 symbols, respectively.

Key words:

wireless communication, channel estimation, MIMO, orthogonal pilot sequences, bit-error rate.

Research article

© 2020, Vadim Romanuke

This is an open access article licensed under the Creative Commons Attribution-NonCommercial-NoDerivatives 4.0 license (<http://creativecommons.org/licenses/by-nc-nd/4.0/>)

INTRODUCTION

In radio, multiple-input and multiple-output (MIMO) specifically refers to a practical technique for sending and receiving more than one data signal simultaneously, over the same radio channel by exploiting multipath propagation. More generally, MIMO is a method for multiplying the capacity of a radio link by using multiple antennas at the transmitter and receiver ends of a wireless communication system [2]. MIMO systems are increasingly being adopted in wireless communication standards, including IEEE 802.11n (Wi-Fi), IEEE 802.11ac (Wi-Fi), HSPA+ (3G), WiMAX, and Long Term Evolution (4G LTE), for the potential gains in capacity they realize when using multiple antennas. Multiple antennas use the spatial dimension in addition to the time and frequency ones, without changing the bandwidth requirements of the system [14].

When multiple transmitter antennas are used, the concept of orthogonal space-time block coding (OSTBC) is employable [4]. An OSTBC subsystem encodes information symbols from a modulator by using, either the Alamouti code [1] for two transmit antennas, or other generalized complex orthogonal codes [11] for three, or four transmit antennas. To know how a signal propagates from the transmitter to the receiver, and represents the combined effect of scattering, fading, and power decay with distance, the channel state information is required. The channel state information makes it possible to adapt transmissions to current channel conditions, which is crucial for achieving reliable communication with high data rates in multi-antenna systems. In the realistic scenario, where the channel state information is not known at the receiver, this has to be extracted from the received signal. The channel estimator can perform this by using orthogonal pilot signals that are prepended to every packet [5]. Compared to a blind approach, where the estimation is based only on the received data, without any known transmitted sequence, the tradeoff is the accuracy versus the overhead. The orthogonal pilot signal approach has a higher overhead than the blind approach, but it achieves a better channel estimation accuracy than the blind approach [16].

However, in practice, orthogonal pilot sequences, from which the channel between the transmitter and receiver is estimated, are limited by the coherence time of the channel. Most importantly, the reuse of pilot sequences of several co-channel cells may create pilot contamination that worsens the MIMO performance [9]. Another problem is that a loss of a symbol in a pilot sequence (due to channel noise and interference) leads to de-orthogonalization. Obviously, the pilot signal de-orthogonalization may also worsen the MIMO performance [3].

MOTIVATION

Orthogonalization is a crucially important property used in wireless communication systems to increase capacity of a radio channel without badly affecting its reliability. In MIMO, orthogonal codes are usually taken from the Hadamard matrix [12], where the first orthogonal sequence of pilot symbols is the sequence of ones. In fact, it is the Walsh function of the zeroth order, which is a function-constant [13]. In particular, Walsh functions are generated from the Hadamard matrix [15], and can be used as well for other transmit antennas.

Walsh functions have a regular structure as they are mirror-symmetrical (considering from the middle of the unit interval on which the functions are defined). Similar binary functions having irregular structures (IS), and constituting orthogonal sets are known also (e. g., see [6]). The eight orthogonal bases of such irregular-structure binary functions (considering the seven non-zeroth-order functions in every basis; the function-constant, which is the zeroth-order function in every basis, is not considered) found by Romanuke [7] were simulated to substitute the respective Walsh functions in wireless communication systems with the code division multiple access (CDMA). It was shown in [8] that these orthogonal sets of binary functions outperform Walsh set, where the bit-error rate (BER) is decreased by 3 % to 5 %. It is naturally assumed that BER in MIMO systems with the orthogonal pilot signal approach might be decreased by using the similar substitution.

The assumption is to be verified on a 2×2 MIMO system with channel estimation, in which two transmit, and two receive antennas, are employed. It is assumed that the channel remains unchanged for the length of the packet (i. e., it undergoes slow fading), and the channel undergoes independent fading between the multiple transmit-receive antenna pairs. Data are modulated by coherent binary phase-shift keying (BPSK) [10]. Then OSTBC by Alamouti is applied to the modulated data and the signal is passed over flat-fading Rayleigh channels [12].

The goal is to estimate the BER performance of a 2×2 MIMO system with channel estimation by the orthogonal pilot signal approach for both the Hadamard and Romanuke orthogonal codes. The case of a symbol loss (or, in other words, a symbol error) in a pilot sequence (that implies a de-orthogonalization) is to be studied as well. For this, various situations are to be considered: de-orthogonalization caused by one and two pilot sequence symbol errors, where subcases of symbol definiteness and repeatability should be simulated.

BPSK-OSTBC SIMULATION PARAMETERS

The simulation is based on MATLAB® R2019a Communications System Toolbox™ functions covering an end-to-end 2×2 MIMO system. The fundamental parameters for simulating BPSK and OSTBC are as follows: frame length F , number of pilot symbols per frame P , bit-energy-to-noise-density ratio (BENDR) $r_{\text{Eb}/\text{No}}$ in dB, maximum number of errors m_{err} , maximum number of packets N_{pack} . The simulation is run over a range of BENDR points to generate BER results that allow comparing different cases.

It is reasonable to vary BENDR from 0 dB to 6 dB with a step of 1 dB. The frame length is equal to 32, 64, 128, 256 symbols. The number of pilot symbols per frame cannot exceed 25 % of the frame length, so it is set according to tab. 1.

Tab. 1. The 10 cases of the parameter pair of the frame length and pilot symbols per frame

F	32	64	128	256	frame length
P	8	8	8	8	number of pilot symbols per frame
	P	16	16	16	
		P	32	32	
			P	64	

For the 2×2 MIMO system, the two Hadamard orthogonal sequences, regardless of the number of pilot symbols per frame, have the view presented in fig. 1. In fact, these are the Walsh functions of the zeroth order and $(P - 1)$ -th order (i. e., the last function in the Walsh basis of functions corresponding to P -positioned orthogonal codes). The IS binary functions (ISBFs) by Romanuke shown in fig. 2 have the same function-constant, so it is better to use the last two functions from each basis of P functions (fig. 3).

The above-mentioned de-orthogonalization occurs when the negative value of a binary function is dropped into the positive value, and vice versa. These pilot sequence symbol errors are notationally referred to as “0→1” and “1→0”, respectively. To estimate the BER performance under circumstances of imperfect orthogonality, the six cases (tab. 2) are to be simulated for both the Hadamard and Romanuke orthogonal codes. The number of BPSK-OSTBC simulations should be sufficiently great for obtaining stable results. The stability of these results is expected to be confirmed by carrying out another series of simulations.

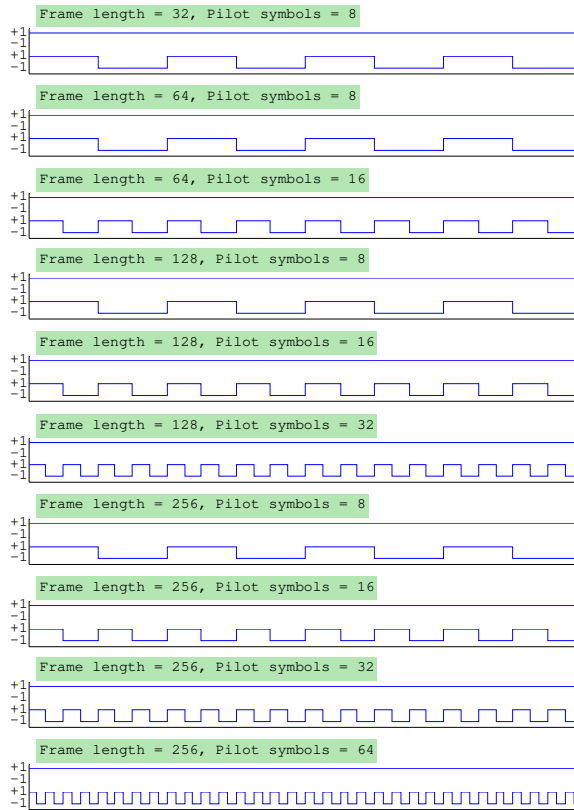


Fig. 1. The two Hadamard orthogonal sequences for different cases of pilot symbols per frame

Tab. 2. The six cases to be simulated

case #	Description	Notation of pilot sequence symbol errors
1	Without de-orthogonalization	there are no pilot sequence symbol errors
2	De-orthogonalization caused by one indefinite pilot sequence symbol error	"0→1" or "1→0"
3	De-orthogonalization caused by one definite pilot sequence symbol error	"0→1"
4	De-orthogonalization caused by two repeated indefinite pilot sequence symbol errors	"0→1" and "0→1" or "1→0" and "1→0"
5	De-orthogonalization caused by two repeated definite pilot sequence symbol errors	"0→1" and "0→1"
6	De-orthogonalization caused by two indefinite pilot sequence symbol errors	"0→1" and "0→1", or "1→0" and "1→0", or "1→0" and "0→1", or "0→1" and "1→0"

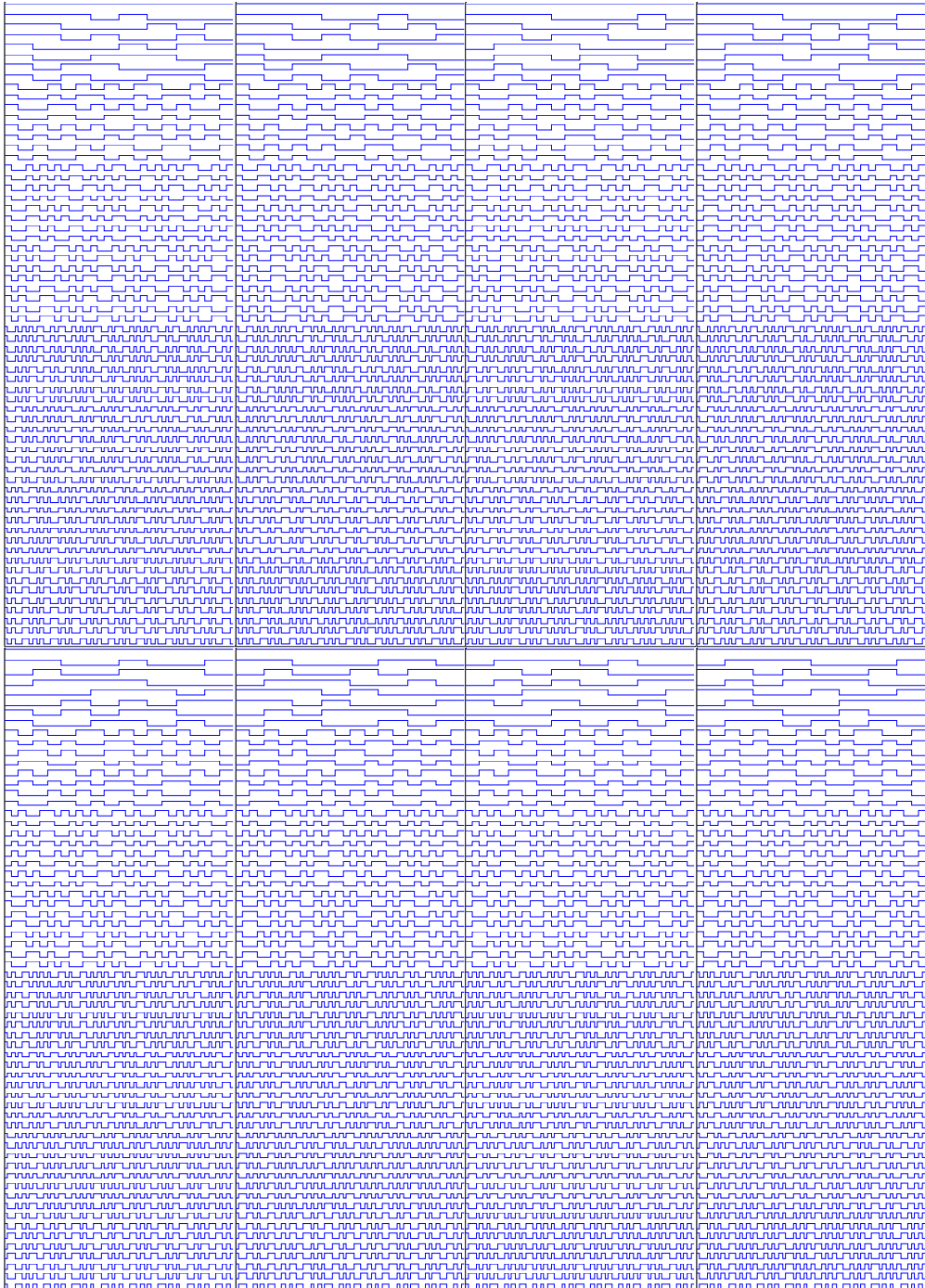


Fig. 2. The eight orthogonal bases presented for the case of 64-positioned orthogonal codes [13]

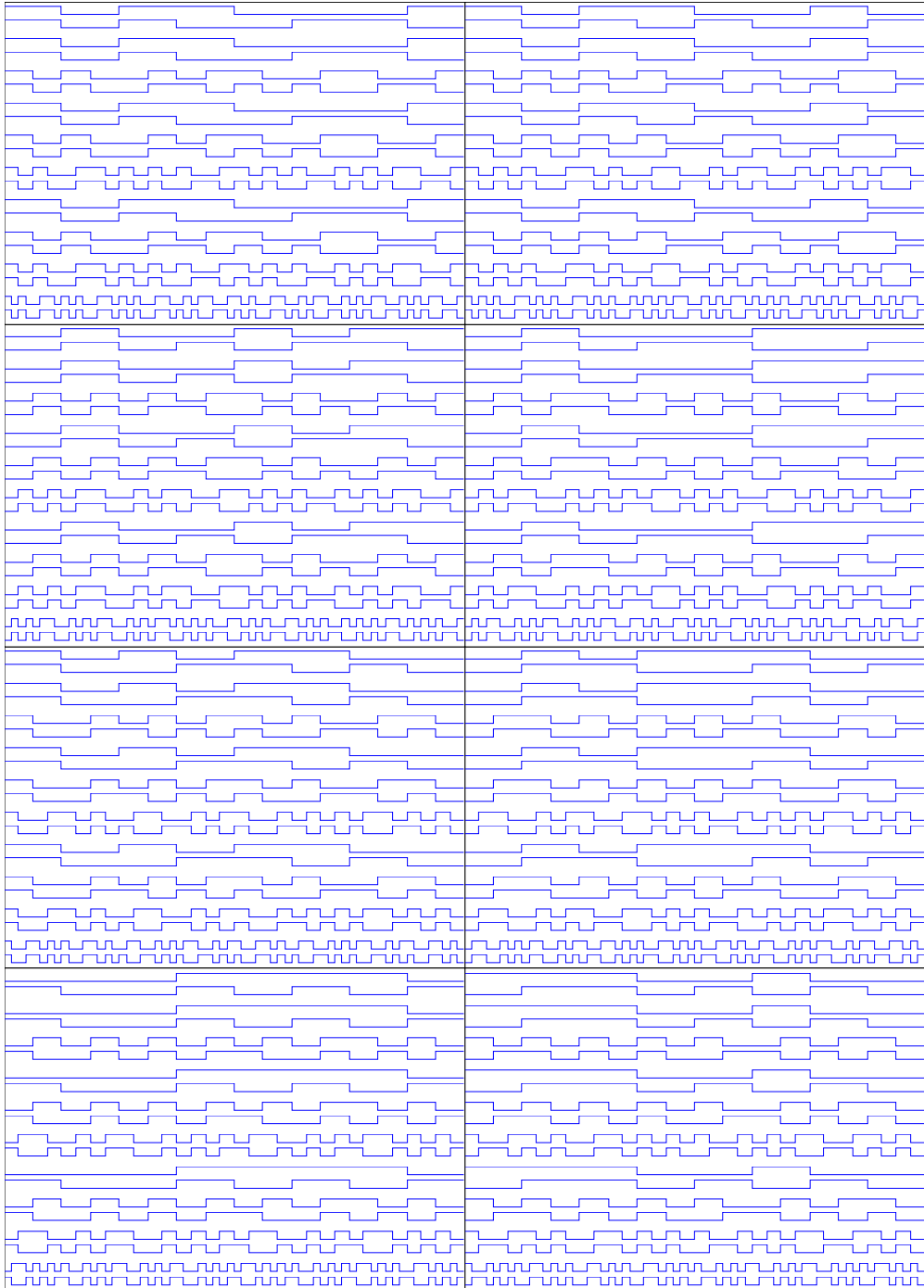


Fig. 3. The last two orthogonal basis-wise sequences for different cases of pilot symbols per frame

To obtain statistically reliable simulation of the 10 cases of pilot symbols per frame and frame length (tab. 1), it is reasonable to set $N_{\text{pack}} = 10m_{\text{err}}$. The two Hadamard orthogonal sequences to be used for the simulation are taken as they are shown in fig. 1. The two IS orthogonal sequences (in each of the eight bases) to be used for the simulation are taken as they are shown in fig. 3.

SIMULATION RESULTS

Considering the perfect orthogonality, i. e. case #1 in tab. 2, the substitution of the Hadamard sequences (fig. 1) for the IS sequences (by ISBFs in fig. 3) gives no gain. The de-orthogonalization caused by one indefinite pilot sequence symbol error (case #2) cannot be rectified by the substitution as well. The BER performance for $N_{\text{pack}} = 500000$ is shown in fig. 4 for this case, where the circled points (IS sequences for the de-orthogonalization case), and squared points (Hadamard sequences for the de-orthogonalization case) are plotted along with the dotted points (IS sequences for case #1) and asterisked points (Hadamard sequences for case #1). The BER performance for $N_{\text{pack}} = 500000$ shown in fig. 5 (with the same point markers, which will be used further) for case #3 is similar to that. Those polylines re-plotted for $N_{\text{pack}} = 250000$ for case #2 (fig. 6) and case #3 (fig. 7) are almost repeated, so the results are statistically consistent and thus reliable. The averaged BER performance for these cases are presented in fig. 8 and fig. 9, where the difference between the perfect orthogonality and de-orthogonalization is clear.

In case #4, the BER performance by the Hadamard sequences is improved by the IS sequences (fig. 10). This improvement is even more obvious for case #5 (fig. 11). Those polylines re-plotted for $N_{\text{pack}} = 250000$ for case #4 (fig. 12), and case #5 (fig. 13) are almost repeated, so the results are statistically consistent, and thus reliable. The averaged BER performance for these cases are presented in fig. 14 and fig. 15. In case #4, the BER is decreased by almost 10 % on average by using the IS sequences. In case #5, the BER is decreased by almost 16 % on average.

In case #6, the BER performance by the Hadamard sequences is improved by the IS sequences (fig. 16), although the improvement is less obvious than in cases #4 and #5. This is confirmed by re-simulating it for $N_{\text{pack}} = 250000$ (fig. 17). On average, the BER is decreased by almost 2.9 % (fig. 18).

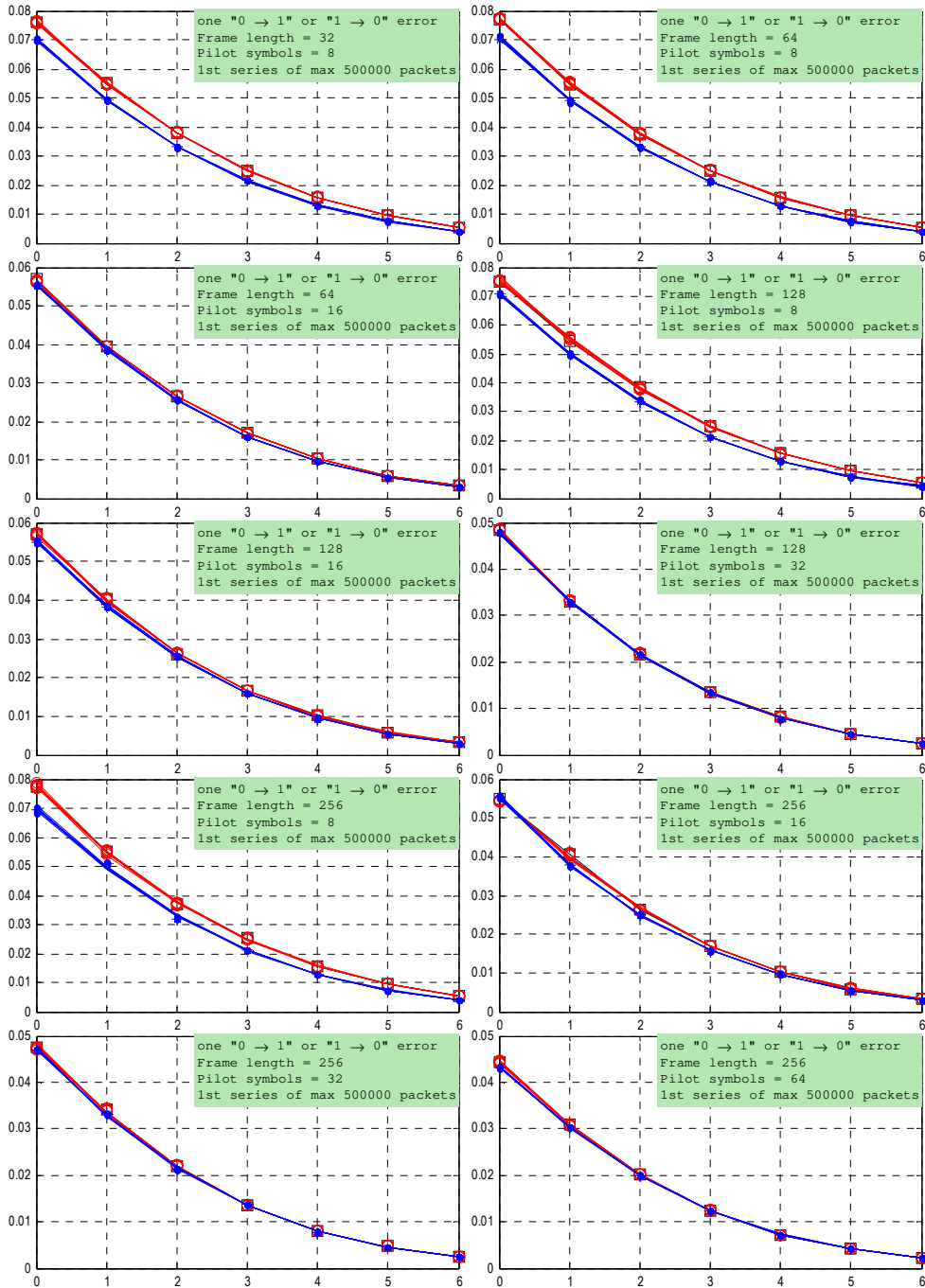


Fig. 4. The BER performance versus BENDR by one indefinite pilot symbol error de-orthogonalization ("0→1" or "1→0") for the first series of maximum 500000 packets

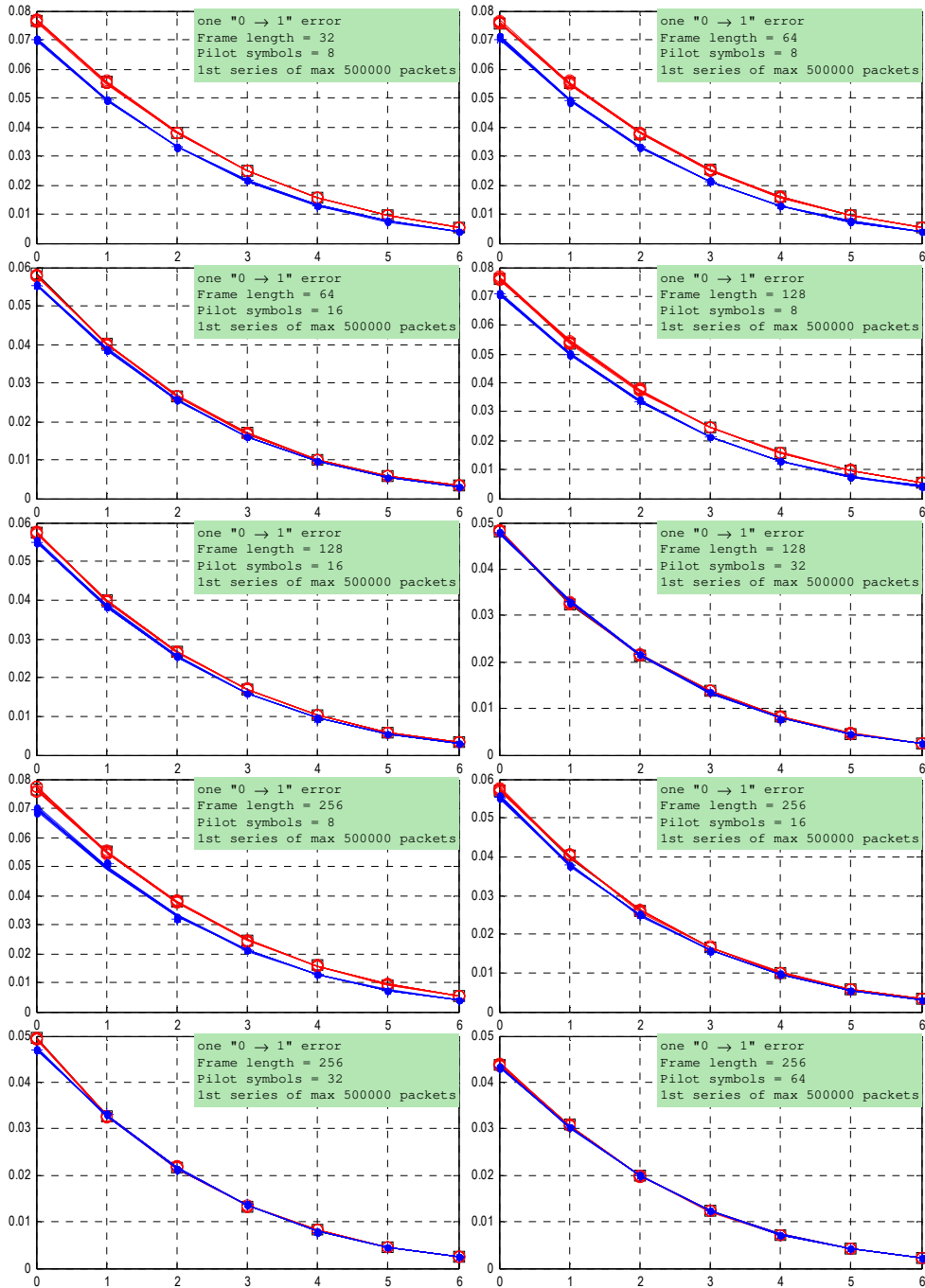


Fig. 5. The BER performance versus BENDR by one definite pilot symbol error de-orthogonalization ("0→1") for the first series of maximum 500000 packets

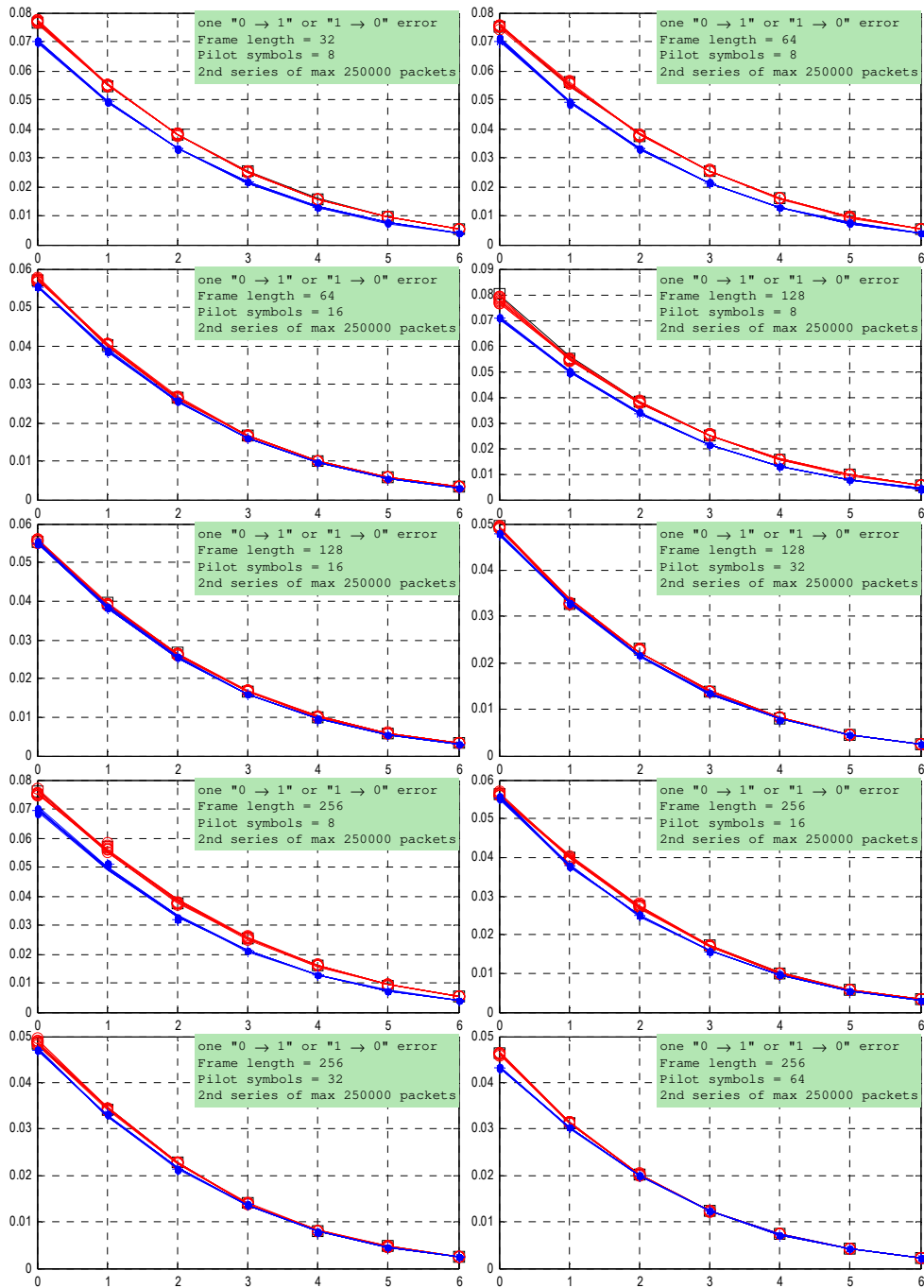


Fig. 6. The BER performance versus BENDR by one indefinite pilot symbol error de-orthogonalization ("0→1" or "1→0") for the second series of maximum 250000 packets

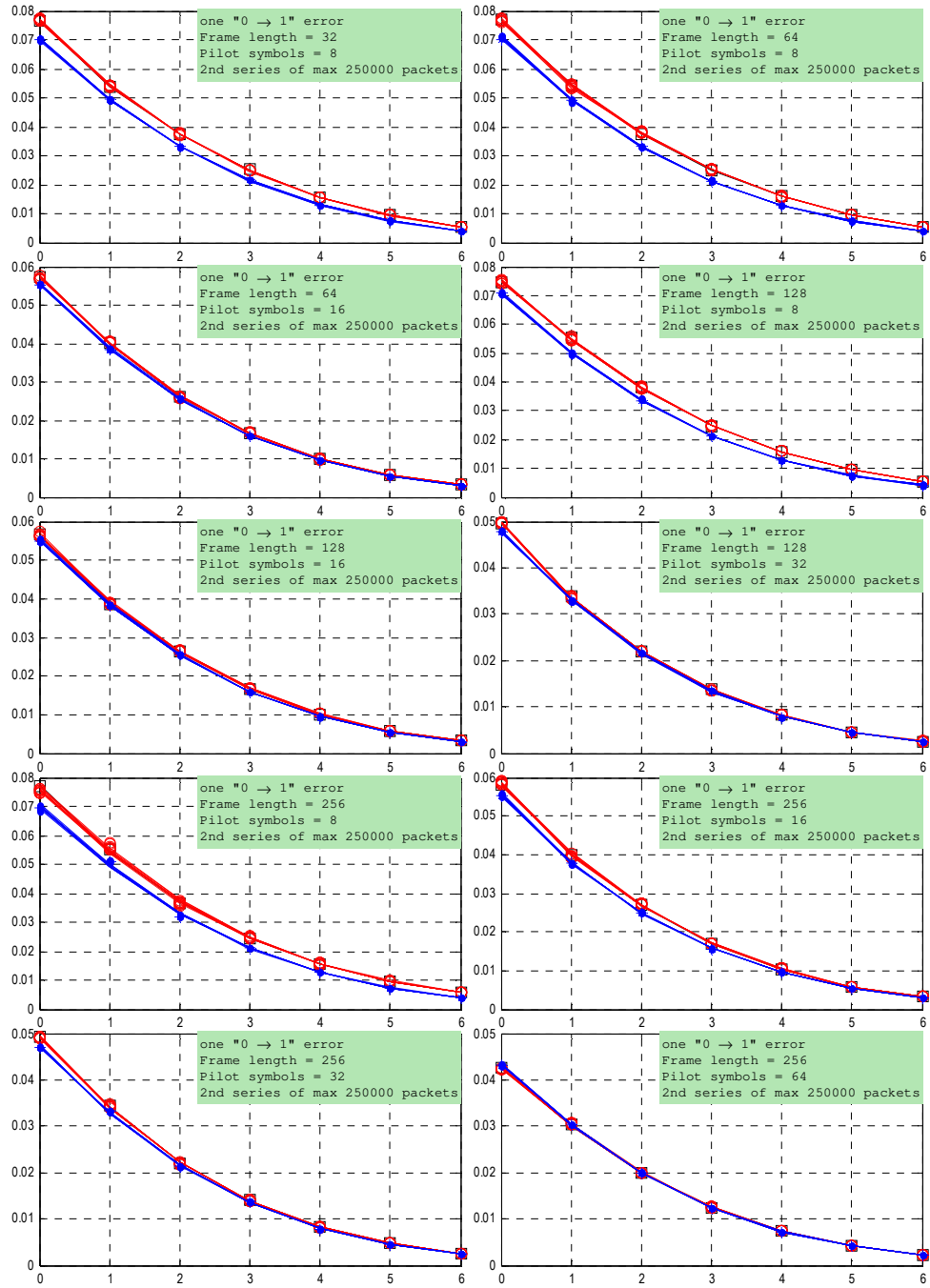


Fig. 7. The BER performance versus BENDR by one definite pilot symbol error de-orthogonalization ("0→1") for the second series of maximum 250000 packets

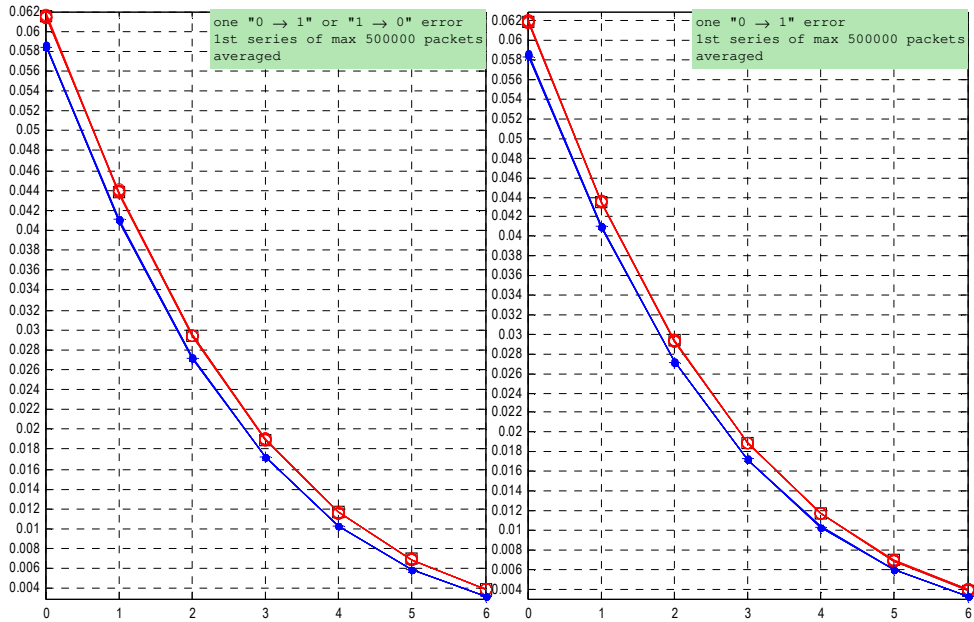


Fig. 8. The averaged BER performance versus BENDR by one pilot symbol error de-orthogonalization (cases #2 and #3) for the first series of maximum 500000 packets

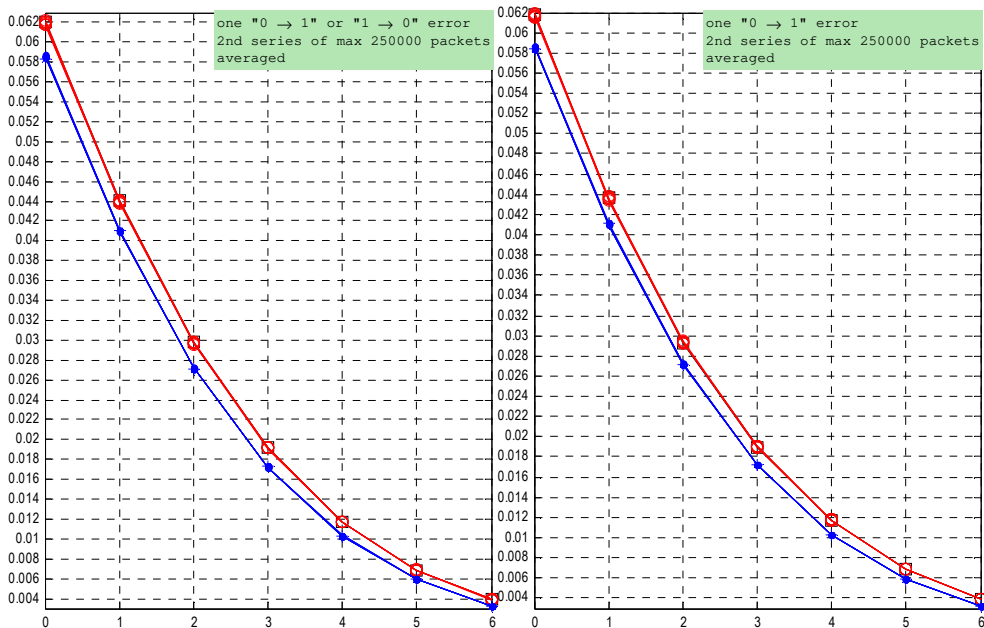


Fig. 9. The averaged BER performance versus BENDR by one pilot symbol error de-orthogonalization (cases #2 and #3) for the second series of maximum 250000 packets

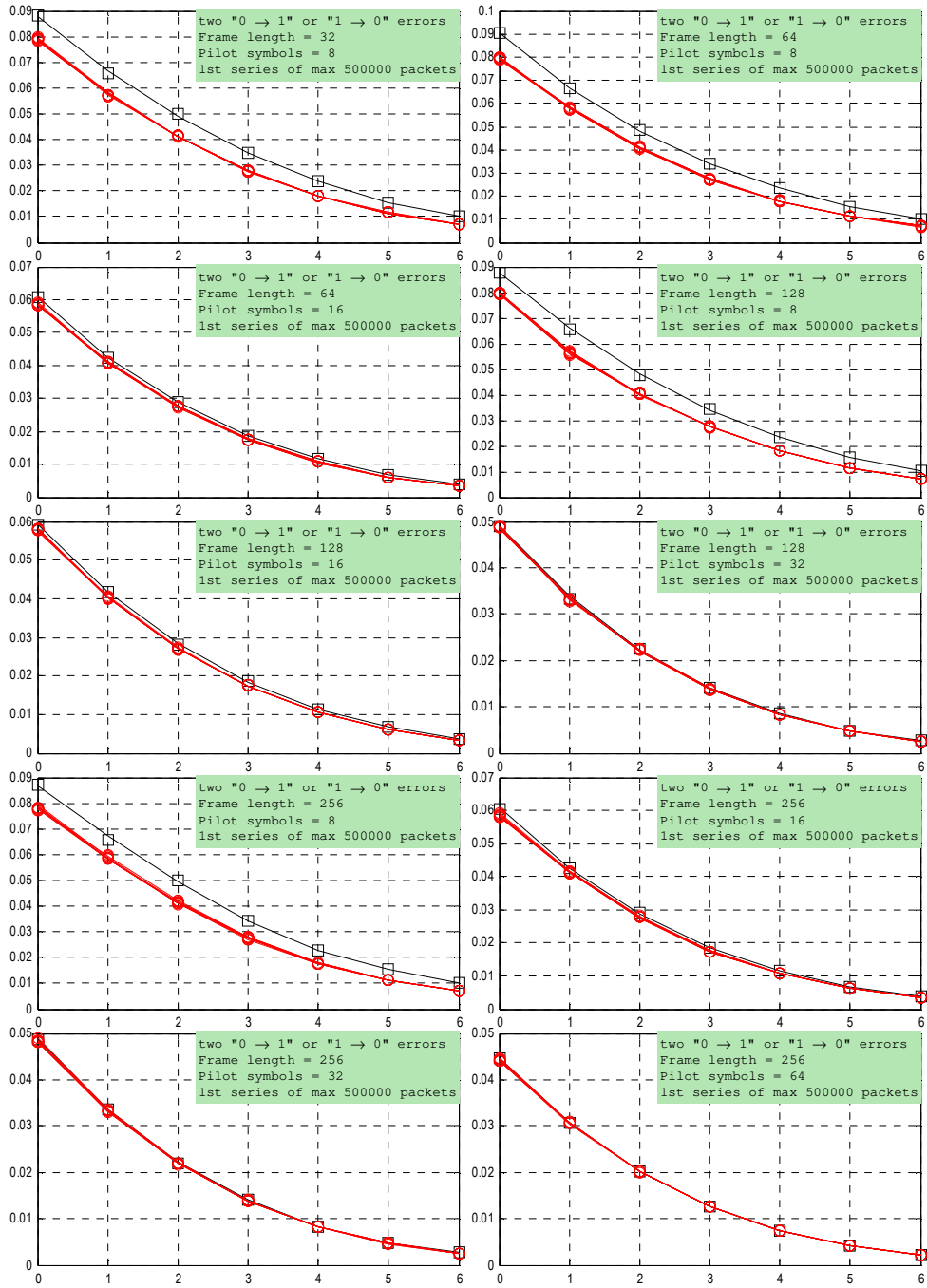


Fig. 10. The BER performance versus BENDR by two repeated indefinite pilot symbol error de-orthogonalization (twice "0→1" or "1→0") for the first series of maximum 500000 packets

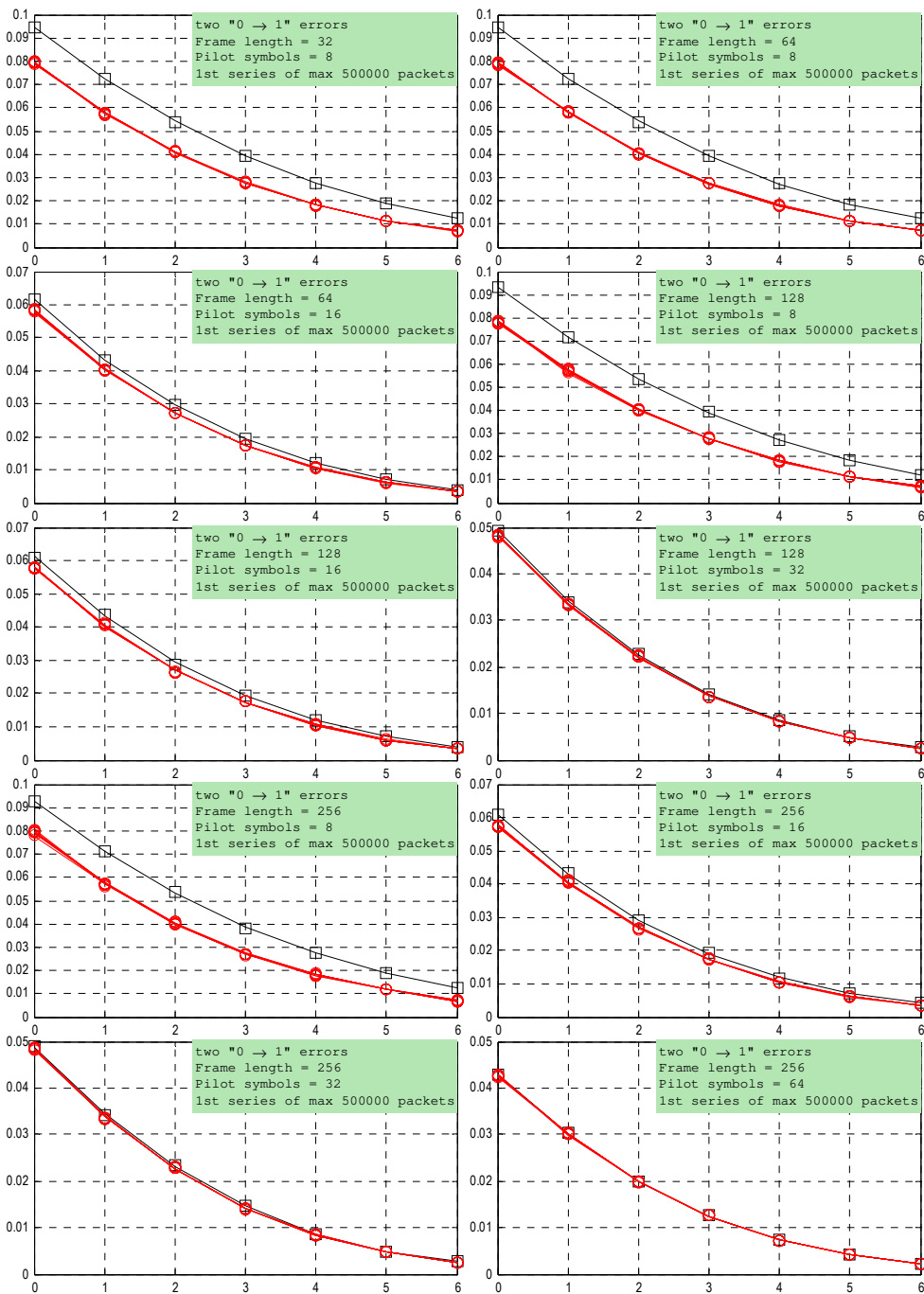


Fig. 11. The BER performance versus BENDR by two repeated definite pilot symbol error de-orthogonalization ("0→1" and "0→1") for the first series of maximum 500000 packets

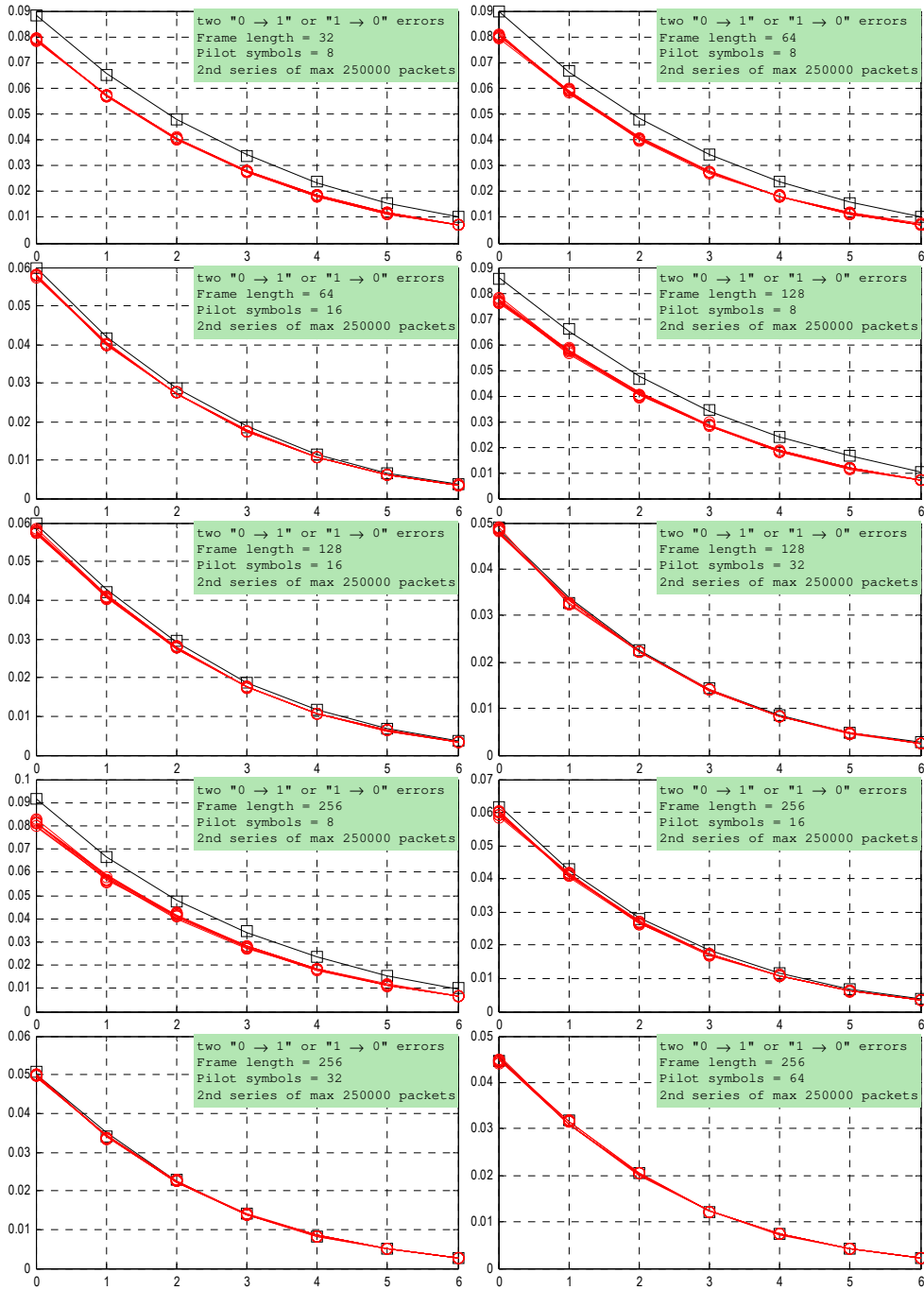


Fig. 12. The BER performance versus BENDR by two repeated indefinite pilot symbol error de-orthogonalization (twice "0→1" or "1→0") for the second series of maximum 250000 packets

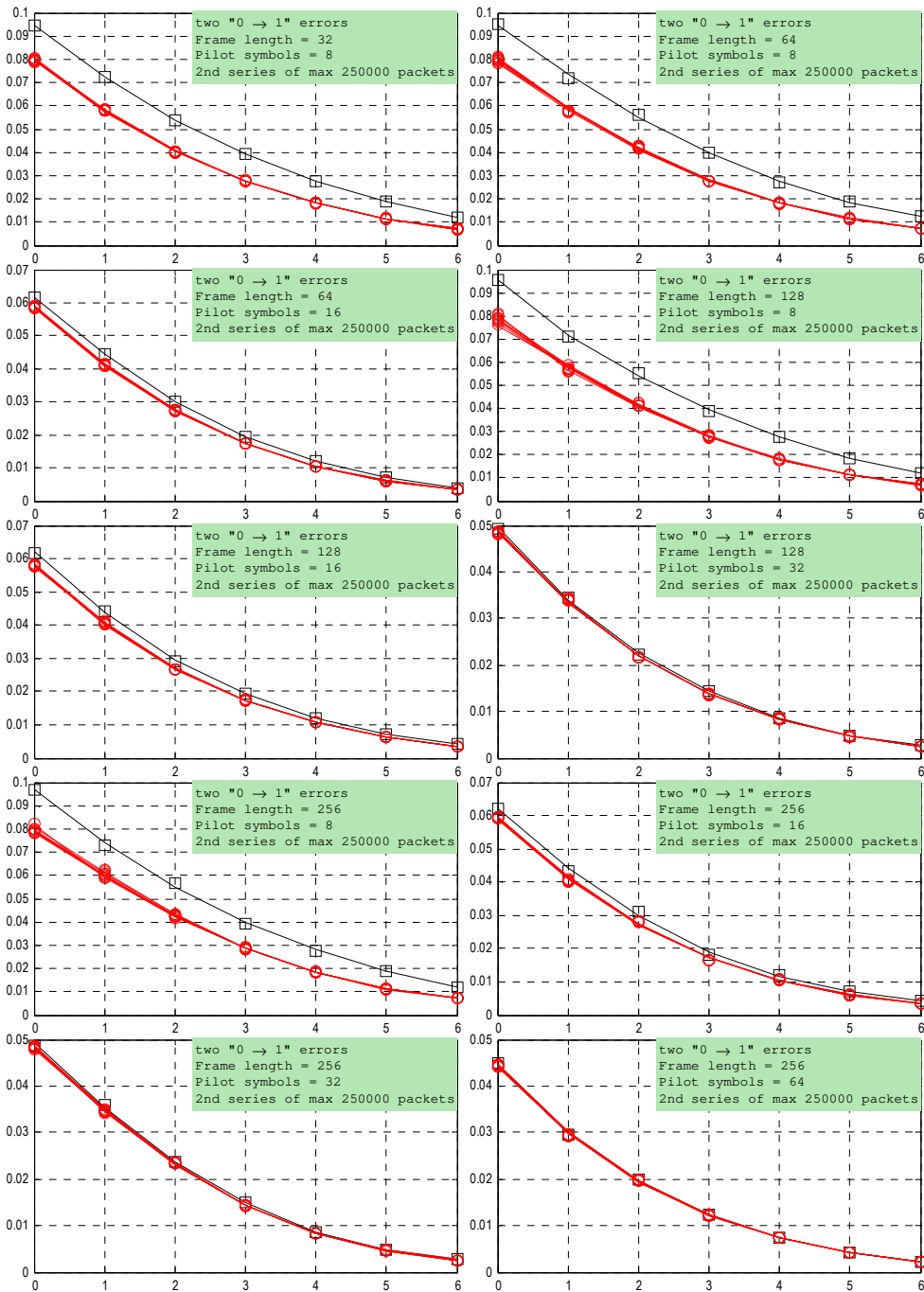


Fig. 13. The BER performance versus BENDR by two repeated definite pilot symbol error de-orthogonalization ("0→1" and "0→1") for the second series of maximum 250000 packets

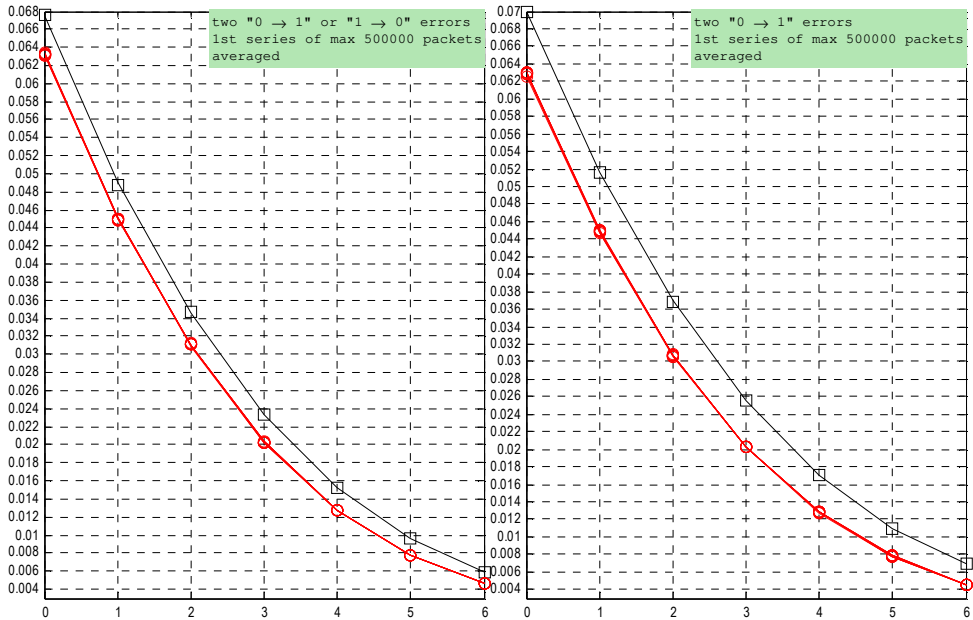


Fig. 14. The averaged BER performance versus BENDR by two repeated pilot symbol error de-orthogonalization (cases #4 and #5) for the first series of maximum 500000 packets

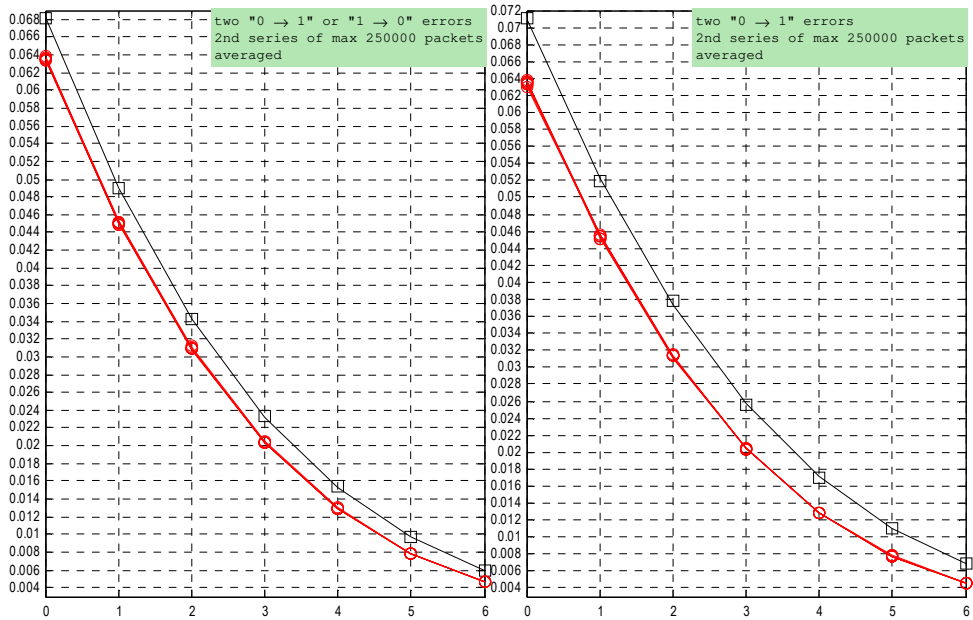


Fig. 15. The averaged BER performance versus BENDR by two repeated pilot symbol error de-orthogonalization (cases #4 and #5) for the second series of maximum 250000 packets

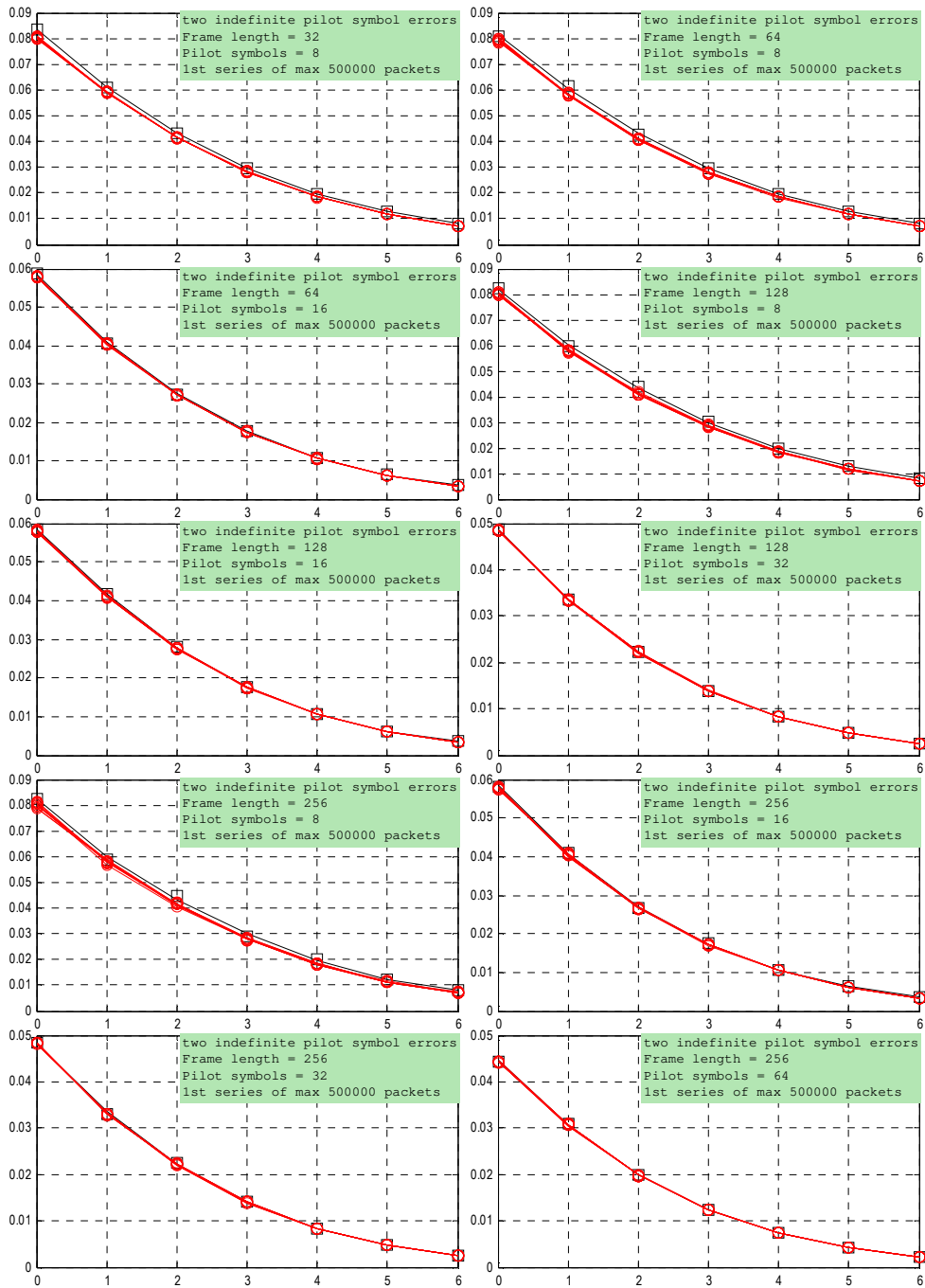


Fig. 16. The BER performance versus BENDR by two indefinite pilot symbol error de-orthogonalization for the first series of maximum 500000 packets

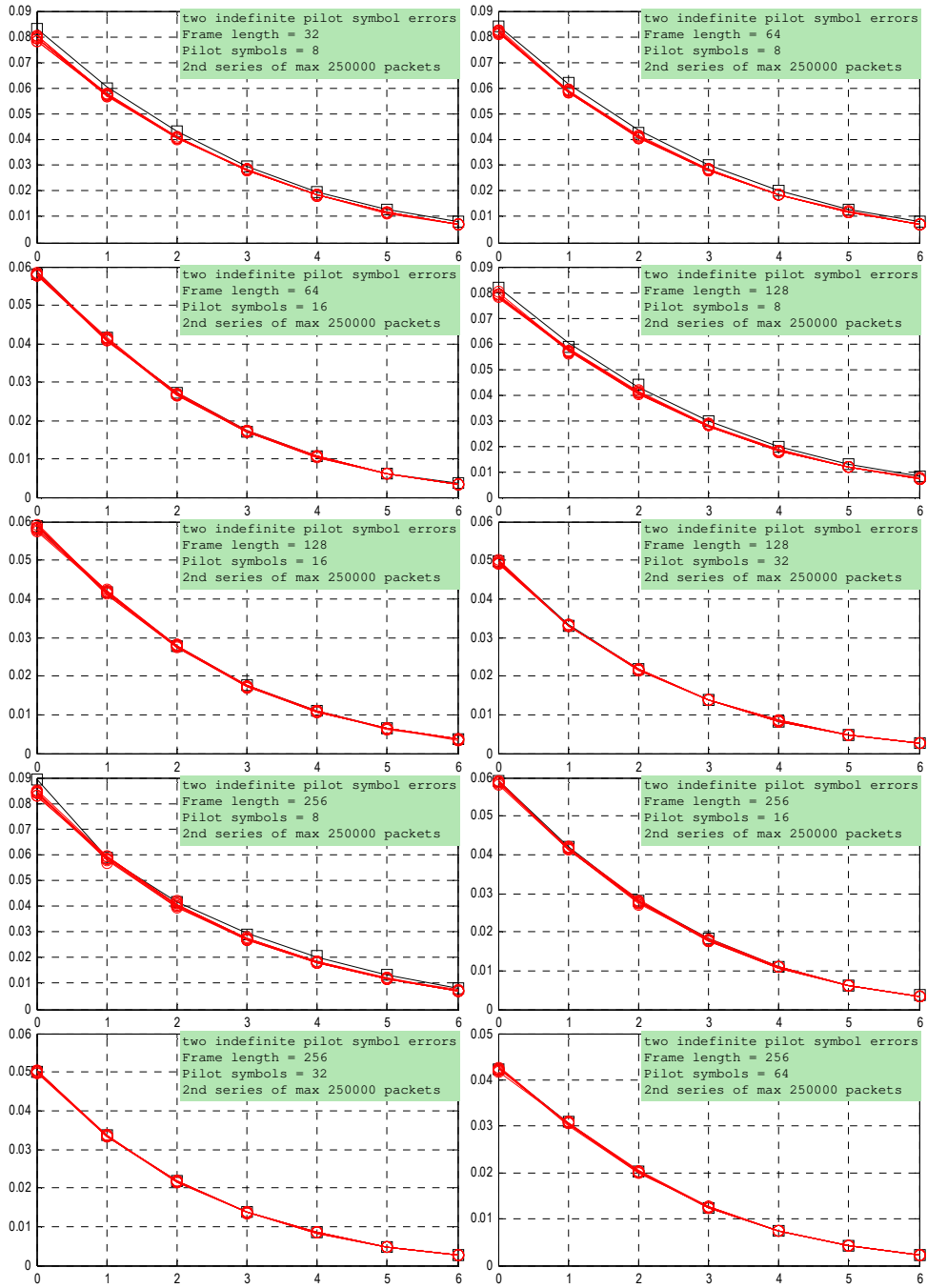


Fig. 17. The BER performance versus BENDR by two indefinite pilot symbol error de-orthogonalization for the second series of maximum 250000 packets

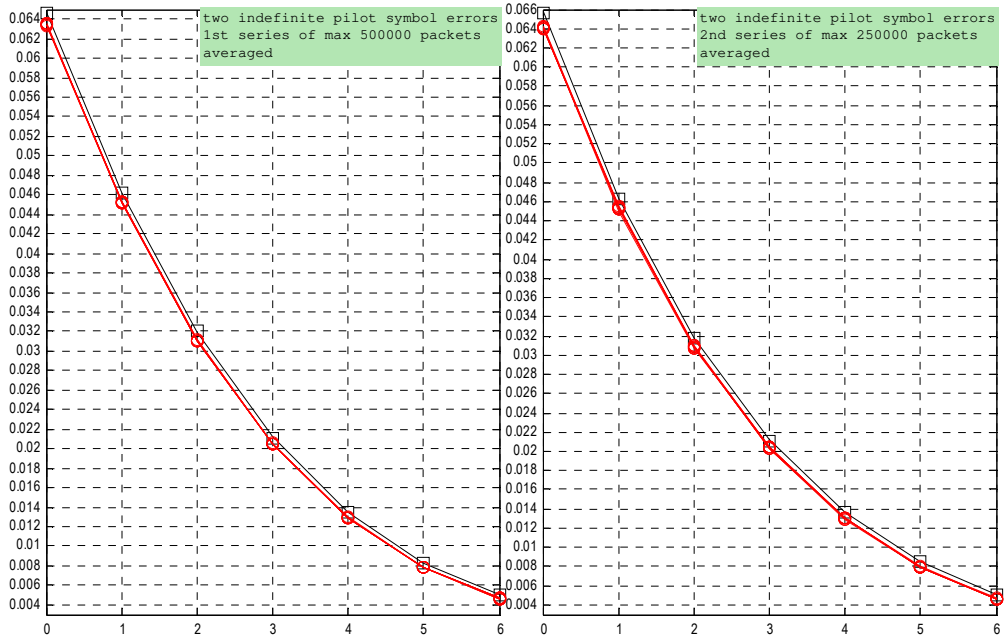


Fig. 18. The averaged BER performance by two indefinite pilot symbol error de-orthogonalization

It is worth noting, that the difference between the BER performance by the Hadamard, and IS sequences in the case of the perfect orthogonality (case #1) may exist. However, this difference is as negligible as it is for the cases (as tagged herein-before, cases #2 and #3) of one pilot symbol de-orthogonalization (fig. 4 – 9). In detail, the difference is not greater than 10^{-5} which is 0.033 %. The one pilot symbol de-orthogonalization still has a negative impact on the BER performance as it then impaired by 0.001 to 0.0035 (see it in both fig. 8 and fig. 9).

DISCUSSION

The polylines in fig. 4 – 7 allow seeing that the BER badly increases for the four following cases of the parameter pair of the frame length and pilot symbols per frame:

$$\{F = 32, P = 8\}, \{F = 64, P = 8\}, \{F = 128, P = 8\}, \{F = 256, P = 8\}. \quad (1)$$

This implies that using 8 pilot symbols in 2x2 MIMO systems, even if it is 25 % of the frame length, has poor efficiency. Thus, the accuracy-versus-overhead tradeoff

herein is unacceptable. Moreover, cases (1) confirm that increasing the frame length does not give necessarily a gain in the BER performance. Indeed, comparison of the respective BER polylines for cases (1) in fig. 4 – 7 reveals that they are almost unchangeable. Noticeable changes are in fig. 10 – 13, but they are not very significant. Weakly-varying polylines for cases (1) are also seen in fig. 16 and fig. 17.

Despite the one pilot symbol de-orthogonalization does have a negative impact on the BER performance, it becomes apparent only for cases (1) and, with less significance, for cases

$$\{F = 64, P = 16\}, \{F = 128, P = 16\}, \{F = 256, P = 16\}. \quad (2)$$

The one pilot symbol de-orthogonalization still increases the BER for cases

$$\{F = 128, P = 32\}, \{F = 256, P = 32\}, \{F = 256, P = 64\} \quad (3)$$

at $r_{\text{Eb}/\text{No}} < 3$ dB, but it is hardly noticeable. The least BER itself is obtained for case

$$\{F = 256, P = 64\} \quad (4)$$

corresponding to a 2×2 MIMO system transferring long frames with a maximum information for channel estimation. This is easily confirmed by fig. 4 – 7, 10 – 13, 16, 17.

By the two repeated pilot symbol error de-orthogonalization, the BER is efficiently decreased by substituting the Hadamard sequences for the IS sequences for cases (1), that is clearly seen in fig. 10 – 13. In the case of the two repeated definite pilot symbol error de-orthogonalization, the gap between the Hadamard sequences polylines (squared points), and IS sequences polylines (circled points) is bigger. Nevertheless, it does not mean that the IS sequences are less effective in the case of the two repeated indefinite pilot symbol error de-orthogonalization. In fact, when the definite symbol is lost twice (in case #5, it is an inversion to the value of the function-constant, i. e., “0→1”), the performance by the Hadamard sequences becomes poorer than that by the IS sequences (compare fig. 10 to fig. 11, and fig. 12 to fig. 13, and also the left subplots to the right subplots in both fig. 14 and fig. 15). The gaps are significantly smaller for cases (2), in the both cases of the two repeated pilot symbol error de-orthogonalization (cases #4 and #5 in fig. 10 – 13). For cases (3), the gaps between the Hadamard sequences and IS sequences polylines are hardly noticeable (without zooming in on the respective polylines). However, some tiny gaps exist just for cases

$$\{F = 128, P = 32\} \text{ and } \{F = 256, P = 32\} \quad (5)$$

whereas there are no gaps for case (4). The same inference is made from fig. 16 and fig. 17 for the two indefinite pilot symbol error de-orthogonalization (case #6). Moreover, the polylines in the respective subplots for cases (3) do not have any difference from the respective polylines (it is better to pay attention to asterisked points) in fig. 4 – 7. Therefore, 2×2 MIMO systems transferring long frames with a maximum information for channel estimation are resistant to partial de-orthogonalization in pilot signals. The accuracy-versus-overhead tradeoff herein is likely to be acceptable.

Surely, in the realistic scenario, the pilot signal de-orthogonalization is highly probable. However, the considered de-orthogonalization cases (tab. 2) are not equiprobable. Considering only one pilot sequence symbol error, case #3 is 50 % probable. If to consider possibility of two pilot sequence symbol errors, cases #2 and #6 are complementary events. They can be counted equiprobable. Consequently, case #3 is then 25 % probable, case #4 is 25 % probable, and case #5 is then 12.5 % probable.

CONCLUSIONS

In 2×2 MIMO systems with channel estimation by the orthogonal pilot signal approach, it is possible to improve the BER performance by substituting the Hadamard sequences for the IS sequences. The improvement is estimated as a BER average decrement. The decrement is almost 10 % in the case of a de-orthogonalization caused by two repeated indefinite pilot sequence symbol errors. The probability of this case is estimated at 25 % rate. In the case of a de-orthogonalization caused by two repeated definite pilot sequence symbol errors, which is 12.5 % probable, the decrement is almost 16 %. Considering two any pilot symbol errors, whose probability is estimated at 50 % rate, the BER is decreased by almost 2.9 %.

Whichever sequences are used for piloting, the 2×2 MIMO system is resistant to the de-orthogonalization if the frame is of 128 to 256 symbols piloted with 32 to 64 symbols, respectively. The accuracy-versus-overhead tradeoff is thus optimized. A further research might be directed towards optimizing MIMO systems in which a greater number of transmit and receive antennas are employed.

REFERENCES

- [1] Alamouti S. M., *A simple transmit diversity technique for wireless communications*, 'IEEE Journal on Selected Areas in Communications', 1998, Vol. 16, No. 8, pp. 1451–1458.
- [2] Berger L. T., Schwager A., Pagani P., Schneider D. M., *MIMO Power Line Communications: Narrow and Broadband Standards, EMC, and Advanced Processing. Devices, Circuits, and Systems*, CRC Press, 2014.
- [3] Han H.-D., Nguyen D.-A., Nguyen V.-D., Nguyen T.-H., Zia M., *Pilot decontamination for multi-cell massive MIMO systems using asynchronous pilot design and data-aided channel estimation*, 'Physical Communication', 2018, Vol. 30, pp. 76–85.
- [4] Larsson E., Stoica P., *Space-Time Block Coding For Wireless Communications*, Cambridge University Press, UK, 2003.
- [5] Naguib A. F., Tarokh V., Seshadri N., Calderbank A. R., *Space-time codes for high data rate wireless communication: Mismatch analysis*, Proceedings of IEEE International Conference on Communications, Montréal, Québec, Canada, 8–12 June 1997, pp. 309–313.
- [6] Romanuke V. V., *Computational method of building orthogonal binary functions bases for multichannel communication systems with code channels division*, Mathematical Modeling and Computational Methods, Ternopil State Technical University, Ternopil, Ukraine, 2006.
- [7] Romanuke V. V., *Generalization of the eight known orthonormal bases of binary functions to the eight orthonormal bases of binary surfaces*, 'Optoelectronic Information-Power Technologies', 2007, No. 2, pp. 263–271.
- [8] Romanuke V. V., *Simulation of code division by applying systems of orthogonal binary functions $\{\text{wal}(w, \theta)\}_{w=0}^{L-1}$ and $\{\text{rom}_u(r, \theta)\}_{r=0}^{L-1}\}_{u=1}^8$ in L-channeled CDMA-system*, 'Herald of Khmelnytskyi National University. Technical sciences', 2008, No. 6, pp. 121–132.
- [9] Salh A., Audah L., Shah N. S. M., Hamzah S. A., *Mitigating pilot contamination for channel estimation in multi-cell massive MIMO systems*, 'Wireless Personal Communications', 2020, Iss. 112, pp. 1643–1658.
- [10] Stern H., Mahmoud S., *Communications Systems*, Pearson Prentice Hall, 2004.
- [11] Tarokh V., Jafarkhani H., Calderbank A. R., *Space-time block codes from orthogonal designs*, 'IEEE Transactions on Information Theory', 1999, Vol. 45, No. 5, pp. 1456–1467.
- [12] Tsoulos G., *MIMO System Technology for Wireless Communications*, CRC Press, 2006.
- [13] Walsh J. L. *A closed set of normal orthogonal functions*, 'American Journal of Mathematics', 1923, Vol. 45, No. 1, pp. 5–24.
- [14] Zheng L., Tse D. N. C. *Diversity and multiplexing: A fundamental tradeoff in multiple-antenna channels*, 'IEEE Transactions on Information Theory', 2003, Vol. 49, Iss. 5, pp. 1073–1096.
- [15] Zhihua L., Qishan Z., *Ordering of Walsh Functions*, 'IEEE Transactions on Electromagnetic Compatibility', 1983, Vol. EMC-25, No. 2, pp. 115–119.
- [16] Zhuang A., Lohan E. S., Renfors M., *Comparison of decision-directed and pilot-aided algorithms for complex channel tap estimation in downlink WCDMA systems*, Proceedings of 11th IEEE Personal and Indoor Mobile Radio Communications (PIMRC), Vol. 2, London, UK, September 2000, pp. 1121–1125.

PONOWNA ORTOGONALIZACJA PO BŁĘDACH SYMBOLI PILOTUJĄCYCH W SYSTEMACH KO- MUNIKACJI BEZPRZEWODOWEJ 2×2 MIMO

STRESZCZENIE

W pracy przedstawiono symulowany system komunikacji bezprzewodowej 2×2 MIMO z oszacowaniem kanału, składający się z dwóch anten nadawczych i dwóch anten odbiorczych. W procesie szacowania kanału zastosowano podejście ortogonalnego sygnału pilotującego z wykorzystaniem sekwencji Hadamarda. Na potrzeby badań symulacyjnych przyjęto modulowanie danych za pośrednictwem spójnego binarnego kluczowania z przesunięciem fazowym, podczas gdy ortogonalny podsystem kodowania bloków czasoprzestrzennych odpowiedzialny był za kodowanie informacji z wykorzystaniem kodu Alamouti. Na podstawie symulacji ustalono możliwość zmniejszenia współczynnika błędnych bitów przez zastąpienie sekwencji Hadamarda sekwencjami należącymi do ośmiu znanych baz ortogonalnych i charakteryzującymi się nieregularnymi strukturami. W przypadku deortogonalizacji wynikającej z dwóch dowolnych błędów symboli sekwencji pilotujących, współczynnik ten został zmniejszony o prawie 2.9 %. Jeśli deortogonalizacje są spowodowane przez dwa powtarzające się błędy symboli sekwencji pilotujących, nieokreślone i określone błędy uległy zmniejszeniu o odpowiednio 10 % i 16 %. Bez względu na to, które sekwencje zostały użyte do pilotowania, wykazano odporność systemu 2×2 MIMO na deortogonalizację w przypadku, gdy ramka zawierała od 128 do 256 symboli, a rozmiar sekwencji pilotującej mieścił się w zakresie od 32 do 64 symboli.

Słowa kluczowe:

komunikacja bezprzewodowa, estymacja kanału, MIMO, ortogonalne sekwencje pilotujące, współczynnik błędnych bitów.



ICE DRIFT IN THE ARCTIC OCEAN

Czesław Dyrzcz 

Polish Naval Academy, Faculty of Navigation and Naval Weapons, Śmidowicza 69 Str., 81-127 Gdynia, Poland, e-mail: c.dyrzcz@amw.gdynia.pl, ORCID ID: 0000-0002-5199-1241

ABSTRACT

The paper presents results of research based on analysis of historical and present studies of the Arctic ice drift. Current information about Arctic ice drift comes from the scientific expedition organized by the Alfred-Wröngener-Institut Helmholtz Centre for Polar and Marine Research (AWI) from Bremerhaven (Germany) in the Arctic Ocean, as a part of the Multidisciplinary drifting Observatory for the Study of Arctic Climate (MOSAiC), coming from the deck of the icebreaker RV "Polarstern". The main purpose of the article was to collect and illustrate information on the phenomenon of ice drift in the Arctic Ocean, considering data from ongoing research during the MOSAiC expedition. The average movement speed of the icebreaker RV "Polarstern" frozen in Arctic ice during the first three legs of the expedition was over 5 Nm/day, which is characteristic of the current data relating to the speed of the Arctic ice drift in the place of research. On the other hand, the article is popular science, and presents the overall characteristics of Arctic ice drift with an indication of the general directions, and speed of its movement. Ice drift speeds in the Arctic can reach exceptionally high values under favorable conditions. The drift of sea ice reaching at its intensity/intensity values close to the limit (dangerous criterion) in these extreme cases is called the "ice river". The speed of "ice rivers" can reach up to 1–2 knots, however, in extreme conditions up to 9 knots. Based on data from the AWI, correlation points were identified between the speed of Arctic ice drift and the speed of winds and atmospheric pressure values.

Keywords:

sea ice drift, Arctic ice drift, MOSAiC

Research article

© 2020 Czesław Dyrzcz

This journal provides immediate open access to its content under the Creative Commons by 4.0 license.

Authors who publish with this journal retain all copyrights and agree to the terms of the above-mentioned [CC BY 4.0 license](#)

INTRODUCTION

The issue of ice drift in the Arctic Ocean has become particularly important recently, with extreme ice sheet melting during the Arctic summer, followed by freezing and movement. One of the problems studied for the current scientific expedition in the Arctic Ocean as part of MOSAiC is the drift of Arctic ice. It is now interesting information coming from the deck of the icebreaker RV "Polarstern", which is the base of the MOSAiC scientific expedition [7, 10, 11]. During the historical period of research, the phenomenon of Arctic ice drift was carried out by many research expeditions, which did not always succeed. In addition, the results of scientific observations gained during each expedition increased our knowledge, and brought new information about these phenomena [2, 4, 6, 7, 8, 9, 10, 11, 14, 16].

According to W. Zakrzewski [16] the phenomenon of ice drift is the constant motion which is caused by the impact of winds, sea currents, and tidal currents on sea ice not permanently connected to the shore, or sea's bottom. The drift of ice in the sea is a complex, but nevertheless completely orderly phenomenon, and the following external forces influence the phenomenon of ice drift: the force of the wind on the surface of the ice; the force of the water on the drifting ice; the Coriolis force; a component gravity force parallel to the surface of the sea; the power of the interaction of ice floes [16]. The movement of ice can reach high values from a few to several knots. An example of the high speed of ice movement is the so-called "ice rivers", where ice masses have been observed to move up to 9 knots [9]. Observation of ice movement in the Arctic Ocean has been going on for centuries. The article will present three expeditions. The first one is the expedition of USS "Jeannette" commanded by lieutenant Georg W. De Long in the years 1879-1881 [14]. The second one is the expedition of the sailing ship "Fram" in Fridtjof Nansen charge of the scientific side in the years 1893-1896 [8]. The third expedition is currently ongoing MOSAiC, which is based on the RV icebreaker "Polarstern" organized by the Alfred Wegener Institute in 2019-2020 [7, 10, 11]. The most important data for the modern estimation of the ice speed in the transpolar zone was provided by the research performed on the RV "Polarstern" [7, 10, 11].

The main purpose of the article was to collect and illustrate information on the phenomenon of ice drift in the Arctic Ocean, taking into account data from ongoing research during the MOSAiC expedition. On the other hand, the article is a popular science, and presents the overall characteristics of Arctic ice drift with an indication of the general directions and speed of its movement. Following methods

were used to achieve the above aim such an analysis of publications and inference. Implementation of the research was based on the historical material gathered by research institutes and present publications. It is worth emphasizing and highlighting the fact that the article is of a cognitive and popular science character.

The remainder of the paper is organized as follows: Section GENERAL CHARACTERISTICS OF SEA ICE DRIFT gives the description of forces influence the phenomenon of ice drift. Section ICE DRIFT RESERCH IN THE ARCTIC OCEAN presents three research expedition in the Arctic Ocean. Section DRIFT OF ICEBREAKER RV "POLARSTERN" IN THE ARCTIC ICE provides Arctic ice drift observation data, along with the meteorological data necessary to analyse the phenomenon. Finally, some discussion, and conclusions are given in last section.

GENERAL CHARACTERISTICS OF SEA ICE DRIFT

The impact of winds, sea currents, and tidal currents on sea ice are not permanently connected to the shore or sea's bottom to be in constant motion, which is called *drift*. The drift of ice in the sea is a complex, but nevertheless completely, orderly phenomenon [16, p. 69]. According to W. Zakrzewski, the following external forces influence the phenomenon of ice drift [16, p. 69–75]:

- the force of the wind on the surface of the ice;
- the force of the water on the drifting ice;
- the Coriolis force;
- a component gravity force parallel to the surface of the sea;
- the power of the interaction of ice floes.

Wind force on ice surface. This is, in most cases, the main force that causes the drift of sea ice. Because the ice protrudes slightly above the sea surface, and in addition, its upper surface is most often uneven, for example, covered with ice floors. The impact of wind on the surface of the ice is considered as: the force causing the wind to friction with a relatively flat surface of the ice; the force of the wind on the ice surface and wind surfaces, and the lateral surfaces of the coastal parts of the ice floors protruding over the side water. In order to understand the impact of wind on the flat surface of the ice at certain limits, it can be assumed that the wind speed of $v_w = 10 \text{ m/s}$ affects an object with an area of $P = 1 \text{ km}^2$ with a force of approximately 403 000 N, which corresponds to approximately 41 100 kG. On the other hand, if

the surface of the ice floe has ice concentrations (irregular surface) covering 10% of the area of the orifice, the wind force is approximately 884 000 N for the above wind, and ice floe surface, equivalent to approximately 90 150 kG. The value of this force is more than twice the value of the wind force on the flat surface of the ice, although ice floors occupy only 10% of the total ice surface [16, p. 69-72]. With high percentages of coverage of the surface of the icebergs, the wind force is up to 10 times higher.

The impact of water on drifting ice. The water in which the ice is submerged inhibits its movement. The drift of sea ice is opposed by the resistance of the submerged part of the ice floe to the water, and therefore its return is directed inversely to the direction of the ice drift. Of course, this force occurs when the speed of ice drift differs from the speed of the water flowing under the ice. The resistance of the submerged part of the ice floe to the water is the result of the frictional resistance forces formed between the lower surface of the flat ice and water, and the force of the frontal lateral resistance of the underwater surfaces of the ice floors, and the lateral surface of the submerged part of the ice floe. The example value of the frictional resistance force for drift ice floes with an area of $P = 1 \text{ km}^2$, and the difference in ice drift speed, and water current speed of $\Delta v = 0,1 \text{ m/s}$ is approximately 101 000 N, corresponding to approximately 10 300 kG [16, p. 72 to 74]. The resistance strength of the drifting ice floss increases significantly with ice rises among drifting ice.

Coriolis force. The Coriolis force acts on drifting ice at a certain drift speed, as on any moving body in a rotating reference system. The value of Coriolis force depends on the ice mass, latitude, and speed of ice drift. Coriolis force value is highest at the pole, so its impact on the drift of ice in the Arctic Ocean has the greatest value, which is directly proportional to the sine of the angle of latitude. Since the speed of ice drift depends on the speed of the wind, the value of Coriolis force also depends on the wind speed. It is the higher in the higher the wind speed [16, p. 74].

Component gravity force parallel to the sea surface. If the water mirror is tilted at a certain angle from the level, which may occur during the wave, the gravity of the ice on the sea surface can be divided into the following two forces: a force perpendicular to the sea surface, and a force parallel to that surface. A component of the force of gravity parallel to the sea surface causes the ice floe to run down on this inclined surface of the sea.

Interaction of ice hearts. During ice drift, there is a continuous movement of ice floes relative to each other, as a result of which ice floes rub against each other, or collide. As a result, ice floes constantly transfer energy, which causes changes in the

direction and speed of movement of individual ice hearts. The strength of mutual interaction of hearts depends on their mass, speed of movement, and ice compactness [16, p. 74].

The power of the interaction of ice floes. During the drift of ice, ice floes are in continuously movement relative to each other, as a result of which the mats rub against each other or collide with each other. As a result, ice floes are constantly transmitting energy to each other, which causes changes in the direction and speed of movement of individual ice floes. The force of the interaction of floes depends on their mass, speed of movement, and the content of the ice [16, p. 74].

Single ice floe drift caused by winds is rare, however, most often sea ice drifts within ice fields of various sizes and compactness. At a certain wind speed, the speed of ice field drift depends on the compactness of the ice, and the smaller it is, the greater the density of the ice. In the presence of high-density sea ice, the direct wind effect is limited to the ice surface, while the water surface is minimally affected; surface wind currents are very weak and do not support ice drift. In addition, the greater the ice density, the greater are the energy losses of individual ice hearts due to heart collisions, which further explains the slower ice floe drift with a high density compared to loose ice or single ice floes [16, p. 77].

The direction of ice field drift does not coincide with the direction of the blowing wind but is directed about 28–31° to the right in the northern hemisphere due to the Coriolis force. The speed of sea ice drift and the sensitivity of their response to changes in wind speed, and direction depends on the mass of ice floes, the shape of their underwater and underwater parts, and ice content. The lighter the floe, and therefore smaller, or made of thinner ice, the faster it will be set in motion by the wind. When the wind stops, the smaller weight floes stop quickly. Large ice floes, as well as made of ice of very thick ice, have a significant mass, are more difficult to set in motion, while after the wind stops, they move much longer compared to parts of low mass. The speed of ice movement is significantly influenced by tidal currents.

Arctic ice drift speeds can be extremely high under favorable conditions. Sea ice drift reaching near its limit/intensity (dangerous criterion) in these extreme cases is called the "ice river". Intense ice drift and "ice river" are understood to mean drift of ice floes not less than 500 m in size at a speed of not less than 0.5 knots. The speed of the "ice river" can reach up to 1-2 knots, however, in extreme conditions up to 9 knots [6]. The phenomenon of "ice rivers" has a local character, and is often not detectable by traditional ice reconnaissance maps or by calculation.

This is mainly due to the small spatial and temporal dimensions of this phenomena, and to the large changes in ice drift speed as a function of time and space. The phenomenon of the "ice river" has not yet been statistically well studied. To date, only about one hundred such cases have been registered. Detection of this phenomenon by ships was often accompanied by critical and/or emergency events [9, p. 192–193]. Ice drifting in the "ice river" at such a high speed is encountered, among others, on the Northern Sea Route, which is part of the Northeast Passage. "Ice rivers" are dangerous ice phenomenon for ships, and even icebreakers, which, in some cases, were unable to resist their impact.

The pack-ice motion process is associated with [13]:

- diverging (the process of loosening drift ice, leading to a decrease in ice density or stress occurring in it). During the ice deformation processes, fractures (figure 1), cracks, leads, and hummocks occur;
- compacting (decreasing the spacing between floes, resulting in increased ice firmness or the formation of stress that can lead to ice deformation). During compacting process, hummocking, ridging, and rifting occur;

shearing (displacement of floes relative to each other, which can cause rotational movement of floes and the formation of cracks filled with compact ice).



Figure 1. Ice break (fracture) observed from the icebreaker RV "Polarstern" on 10 May 2020 separating part of the "ice camp" from the base

(Source: photo by Christian Rohleder/Alfred-Wegener-Institut.)

ICE DRIFT RESEARCH IN THE ARCTIC OCEAN

Observation of ice mass movement in the Arctic Ocean, and scientific research of this phenomenon have been conducted for a long time. The article will present three expeditions bringing significant value to this issue:

1. Expedition of USS "Jeannette" commanded by lieutenant Georg W. De Long in the years 1879–1881;
2. Expedition of the sailing ship "Fram" in Fridtjof Nansen charge of the scientific side in the years 1893–1896;
3. Currently ongoing MOSAiC expedition based on the RV icebreaker "Polarstern" organized by the Alfred Wegener Institute in 2019–2020.

The steam and sailing ship USS "Jeannette" sailed under the command of lieutenant Georg W. De Long in 1879 to the Arctic Ocean to reach the North Pole and discover unknown water spaces. The expedition ended with the destruction by ice and sinking of the USS "Jeannette" in June 1881 (figure 2), and death of a large part of the 33-man crew. Three years after the sinking of the USS "Jeannette", its remains were discovered on an ice floe near Julianehaab in southwestern Greenland. This floe with debris moved with the powerful polar current from the Novosibirsk Islands, passing from the north of the islands the Land of Franz Josef, Spitsbergen, most likely around the North Pole, and then along with the East Greenland current along the eastern coast of Greenland to Cape Farvel, and beyond west. The distance from the Novosibirsk Islands to Julianehaab along the route shown is approximately 2 900 nautical miles. The remains of the USS "Jeannette" traveled this route in 1 100 days, which indicates an average travel speed of 2.6 NM/day [8].



Figure 2. Destroyed by Arctic ice and sinking USS "Jeannette" in position north-east of the Novosibirsk Islands in June 1881

(Source: USS "Jeannette", Log Book of the United States Navy, Naval History Homepage.)

The MOSAiC expedition was preceded 127 years ago by the expedition of the Norwegian polar explorer Fridtjof Nansen, who set off on a long-term research expedition of the Arctic Ocean on a wooden sailing ship "Fram" (figure 3). The drift in the Arctic ice lasted from September 1893 to 1896. The purpose of the expedition of Fridtjof Nansen was to study the surrounding north pole of the basin on the route from the Novosibirsk Islands, as far north as possible, and then drift in the polar ice to the northwest [7].



Figure 3. Drifting Norwegian sailing ship "Fram" in the ice of the Arctic Ocean during the Fridtjof Nansen expedition in the years 1893-1896

(Source: MOSAiC [8].)

In September 2019, the icebreaker RV "Polarstern" began an annual research expedition in the North Pole area called MOSAiC, and from October 4, 2019, after taking position, it drifts along with polar ice. The ship was built in 1982 in Kiel and Rendsburg (Germany). Basic unit data: length 117.91 m, width 25.07 m, draft 11.21 m, displacement 17 277 t, 4 diesel engines with a total power of 19 000 HP (14 000 kW), speed 15.5 knots. The ship is a research icebreaker ran by Alfred Wegener Institute (AWI) from Bremerhaven. The icebreaker is mainly used for research in the Arctic and Antarctic. During this largest research project in recent years, multidisciplinary studies of the atmosphere, sea ice, oceanography, ecosystem, and bio-chemical will be conducted. Observations are expected to reflect the complex mechanisms associated with climate change.

MOSAiC is the first year-long expedition to the central part of the Arctic Ocean, exploring the Arctic climate system. The project was prepared by an international consortium of leading polar research institutes, led by AWI. Around the icebreaker frozen in ice, research stations are located within a radius of several dozen kilometers. In addition, data is collected by research planes and vessels co-

operating as part of the expedition. Research conducted with such impetus will allow a better understanding of Arctic climate change, and its contribution to global warming.

The first leg of the MOSAiC research expedition was completed on December 16, 2019 with the replacement of the research team, and icebreaker crew members. The exchange and supply took place through the Russian icebreaker "Captain Dranitsyn", who approached the RV "Polarstern" on December 13, 2019, and the break-off of icebreakers took place on December 18, 2019. The second leg was continued in the conditions of polar winter, that is, the darkest and coldest period in the Arctic. On December 29, 2019, the air temperature dropped to below -33°C , and the felt temperature was around -50°C . In mid-November, the research area of the "Polarstern" icebreaker was in the presence of storm winds reaching a speed of about 25 m/s, which affected the deployed equipment in the "ice camp" [7, 10, 11].



Figure 1. Icebreaker RV "Polarstern" drifting with ice of the Arctic Ocean. Visible rifted ice and ridges covered by snow on April 16, 2020

(Source: photo by Michael Gutsche/Alfred-Wegener-Institut.)

During the research expedition MOSAiC, the icebreaker RV "Polarstern" together with the "measuring town/ice camp", set up on ice outside the icebreaker are subjected to drift and processes of occurring deformation of the Arctic ice. Fractures and cracks were observed during the initial phase of the trip. The Arctic winter period was characterized by the creation of hummocking with rifted ice and ridges. As the distance from the North Pole and the changing season of the year started, the deformation process with fracturing was seen.

DRIFT OF ICEBREAKER RV "POLARSTERN" IN THE ARCTIC ICE

The beginning of the icebreaker RV "Polarstern" drift after reaching the starting position for research ($\varphi = 85^{\circ}\text{N}$ and $\lambda = 137^{\circ}\text{E}$) on October 4, 2019, began drifting in the Arctic ice field. The drift was interrupted in connection with the exchange of scientists and crew on May 16, 2020, in position ($\varphi = 83^{\circ}\text{N}$ and $\lambda = 009^{\circ}\text{E}$), and the ship went to the region of the Svalbard. Exiting the ice, and then returning to the Arctic again, was due to the procedure followed in connection with COVID-19 for another research leg. Figure 5 presents the drift route of the icebreaker RV "Polarstern" in the Arctic ice from October 4, 2019 to May 16, 2020, along with the expected further direction of movement as part of the MOSAiC research expedition [7, 10, 11].



Figure 2. Drift route of the icebreaker RV "Polarstern" in the Arctic ice from October 4, 2019 to May 16, 2020 along with the expected further direction of movement as part of the MOSAiC research expedition

(Source: own study [2] based on items provided by AWI [7, 10, 11].)

Based on the AWI data, the daily drift data for the RV icebreaker "Polarstern" from October 4, 2019 to May 16, 2020 is shown in figure 6.

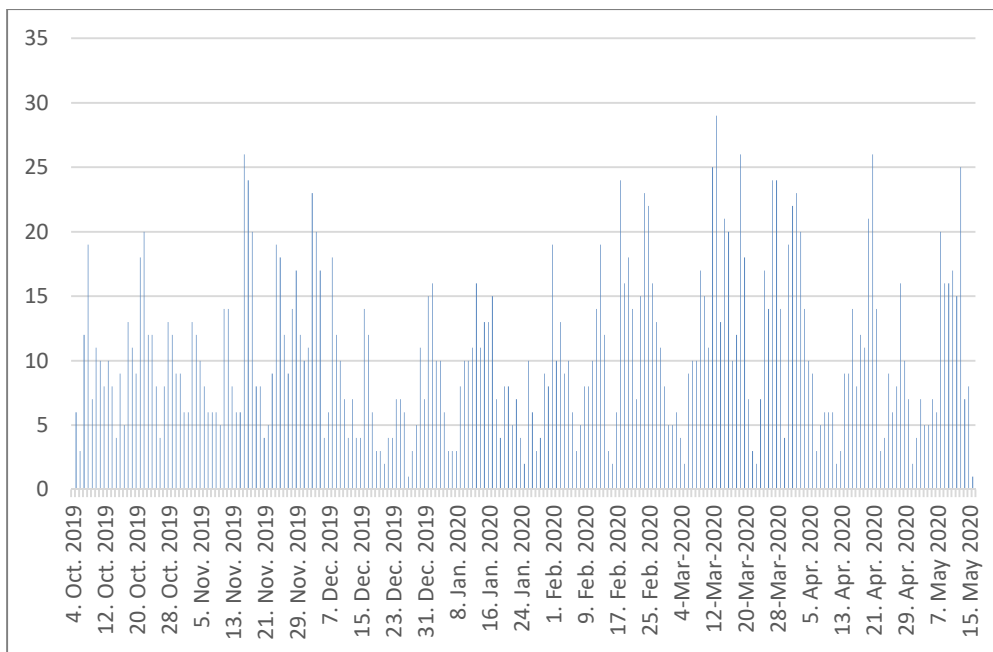


Figure 3. Daily drift of the icebreaker RV "Polarstern" from 4 October 2019 to 16 May 2020 in kilometres (km)

(Source: daily drift information based on AWI data studies [7].)

Meteorological data from RV "Polarstern" with marked values of wind direction, wind speed, barometric pressure, and daily drift in Arctic ice are shown in figure 7. By analyzing and comparing the data collected in figure 7, it can be concluded that the maximum wind speeds associated with low pressure, or a rapid change in atmospheric pressure affect the high sea ice drift values day, or some days after maximums of these data.

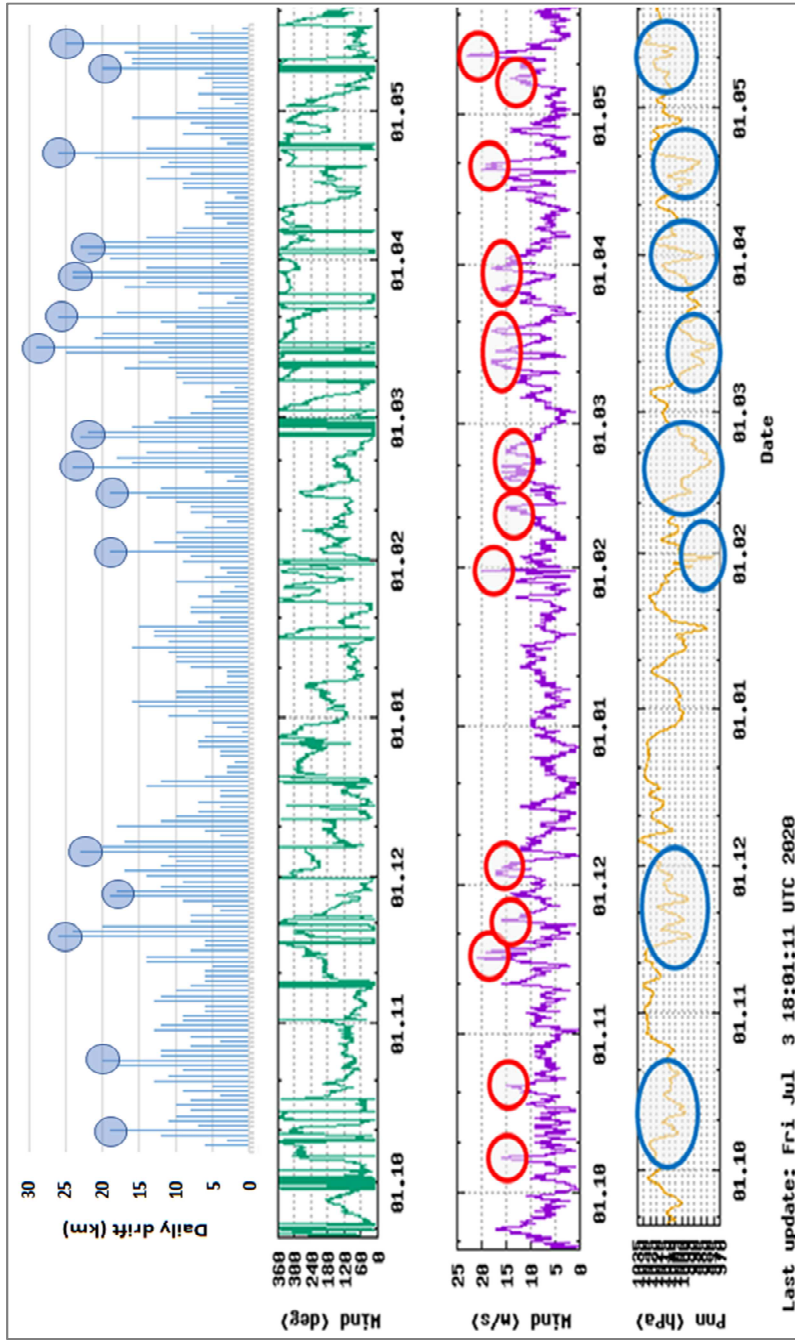


Figure 4. Meteorological data from RV "Polarstern" with marked values of wind direction, wind speed, and barometric pressure with daily drift value in Arctic ice

(Source: Current Meteorological Data AWI [7, 10])

Within 225 days of October 4, 2019 at 01.00 PM to 16 May 2020 at 01.00 AM the German icebreaker RV "Polarstern", together with the "ice research town/ice camp", sailed 2 335 km. **The average daily road was about 10.4 km/day (about 5.6 NM/day or about 0.23 knots).**

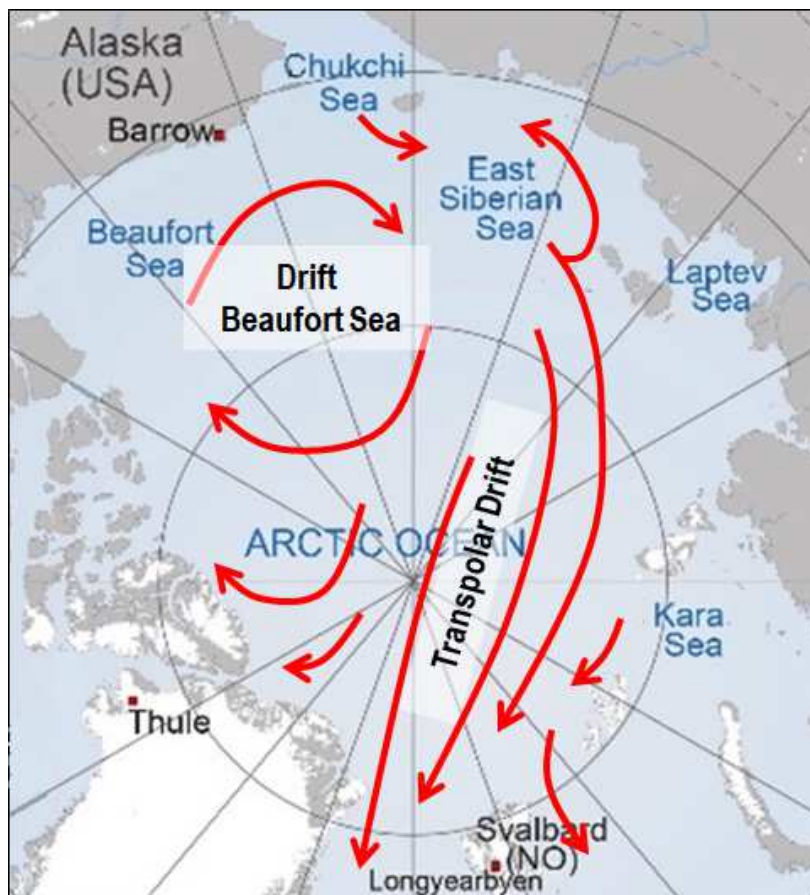


Figure 5. Ice pack drift in the Arctic Ocean

(Source: own study [2].)

The ice of the Arctic Ocean is in a constant drift. The direction and speed of the drift depend on wind conditions, and sea currents. Earlier studies of ice field drift in the Arctic Sea have determined its general course. There are two basic arctic ice circulation systems: Transpolar Drift (Arctic Drift), and Beaufort Sea Drift (Pacific Whirlpool), which are illustrated in Figure 8. Knowledge of ice conditions,

and the phenomena associated with their movement is important for the safety of navigation in the Arctic.

DISCUSSION AND CONCLUSIONS

In the conclusion of the analysis were made of the following generalizations:

1. The following external forces influence the phenomenon of ice drift: the force of the wind on the surface of the ice, the force of the water on the drifting ice, the Coriolis force, the component gravity force parallel to the surface of the sea, and the power of the interaction of ice floes. The article mainly indicates the impact of external forces (wind) on the movement of ice masses.
2. Within 225 days of research expedition the German icebreaker RV "Polarstern" together with the "ice research town/ice camp" sailed 2,335 km, which gives the average daily road about 10.4 km/day (about 5.6 NM/day or about 0.23 knots).
3. Moving along with the RV "Polarstern" ice confirmed the previously accepted because of research and observation of the direction of movement of the Arctic ice. The influence of external forces on ice has a decisive influence on the direction. The article indicates the influence of wind, and other factors were not considered.
4. Comparing the speed of the RV "Polarstern" (5.6 NM/day), and the research sailing vessel "Fram" (2.6 NM/day), one conclude that the RV "Polarstern" was traveling at more twice the speed on its road section. It can be assumed that the speed of travel probably had the thickness of ice at that time, however this thesis needs to be checked. Author does not undertake to answer this problem.

ACKNOWLEDMENT

The author extends special thanks to the Alfred-Wrgener-Institut Helmholtz Centre for Polar and Marine Research (AWI) from Bremerhaven (Germany) for permission to the use of data and images from the deck of the RV icebreaker

"Polarstern" carrying out the Multidisciplinary drifting Observatory for the Study of Arctic Climate (MOSAiC) in the Arctic Ocean.

REFERENCES

- [1] Bowditch N., *The American Practical Navigation*, National Geospatial-Intelligence Agency, Skyhorse Publishing, 2013.
- [2] Dyrzc C., *Dryf lodu morskiego*, preprint for „Nautologia” No 157, Polskie Towarzystwo Nautologiczne, Gdynia 2020 [available in Polish].
- [3] Dyrzc C., *Meteorology and oceanology. Terms, definitions and explanations, 2nd Edition*, Polish Naval Academy, Gdynia 2019.
- [4] Łomniewski K., *Oceanografia fizyczna*, Państwowe Wydawnictwo Naukowe, Warszawa 1969 [available in Polish].
- [5] Marchenko N., *Russian Arctic Seas. Navigational conditions and accidents*. Springer-Verlag, Berlin-Heidelberg 2012.
- [6] Mironov E. U., *Opasnye ledovye javlenija dlja sudochodstva v Arktike*. AANII, St. Petersburg 2010.
- [7] *MOSAiC* - <https://follow.mosaic-expedition.org/> [access: 5 July 2020].
- [8] Nansen F., *Fram w Arktyce*, Wydawnictwo SEL, Kraków 2011 [available in Polish].
- [9] Pastusiak T., Styszyńska A., *Intensywny dryf lodu w rejonie wyspy Wrangla, zjawiska z nim zwiqzane i konsekwencje dla żeglugi*, „Problemy Klimatologii Polarnej, Nr 23, 2013 p. 191–204 [available in Polish].
- [10] *Research ice breaker Polarstern. Current Meteorological Data* - <https://www.awi.de/nc/en/science/long-term-observations/atmosphere/polarstern.html> [access: 5 July 2020].
- [11] *RV Polarstern* - <https://mosaic-expedition.org/expedition/polarstern/> [access: 8 May 2020].
- [12] *Sea-Ice Information Services in the World*, WMO-No. 574, World Meteorological Organization, Geneva, Edition 2017.
- [13] *Sea Ice Nomenclature*, Summary and Purpose of Document WMO No. 259, 5th Session of JCOMM Expert Team on Sea Ice, March 2014.
- [14] Sides H., *W królestwie lodu. Tragiczna wyprawa polarna USS Jeannette*, Dom Wydawniczy REBIS, Wydanie I, Poznań 2016 [available in Polish].
- [15] *USS „Jeannette”*, Log Book of the United States Navy, Naval History Homepage, http://www.naval-history.net/OW-US/Jeannette/USS_Jeannette.htm [access: 14 May 2020].
- [16] Zakrzewski W., *Lody na morzach*, Wydawnictwo Morskie, Gdańsk 1982 [*Ice on the seas* – available in Polish].

DRYF LODU NA OCEANIE ARKTYCZNYM

STRESZCZENIE

W artykule przedstawiono wyniki badań opartych na analizie historycznych i obecnych badań dryftu lodu arktycznego. Aktualne informacje na temat dryftu lodu arktycznego pochodzą z wyprawy naukowej zorganizowanej przez Alfred-Wegener-Institut (AWI) Centrum Badań Polarnych i Morskich z Bremerhaven (Niemcy) na Oceanie Arktycznym w ramach multidyscyplinarnego obserwatora dryfującego klimatu arktycznego (MOSAIc) pochodzącego z pokładu lodołamacza RV „Polarstern”. Głównym celem tego artykułu było zebranie i zilustrowanie informacji o zjawisku dryftu lodu na Oceanie Arktycznym, z uwzględnieniem danych z bieżących badań podczas wyprawy MOSAIc. Średnia prędkość ruchu lodołamacza RV „Polarstern” wraz z lodem arktycznym podczas pierwszych trzech etapów wyprawy wyniosła ponad 5 Nm/dobę. Z drugiej strony, artykuł ma charakter popularnonaukowy i przedstawia ogólną charakterystykę dryftu lodu arktycznego ze wskazaniem generalnych kierunków i prędkości jego ruchu. Prędkości dryftu lodu w Arktyce mogą osiągnąć wyjątkowo wysokie wartości w sprzyjających warunkach. Dryf lodu morskiego osiągający wartości natężenia/intensywności bliskie granicy (niebezpieczne kryterium) w tych ekstremalnych przypadkach nazywa się „lodową rzeką”. Prędkość „lodowych rzek” może osiągnąć do 1–2 węzłów, jednak w ekstremalnych warunkach do 9 węzłów. Na podstawie danych z AWI zidentyfikowano punkty korelacji między prędkością dryftu lodu arktycznego a prędkością wiatru i wartościami ciśnienia atmosferycznego.

Słowa kluczowe:

dryf lodu morskiego, dryf lodu arktycznego, MOSAIc

Editorial Policy

The Editor-in-Chief of the Journal and editors are knowledgeable and qualified in the field of study and are solely and independently responsible for deciding which of the articles submitted to the journal should be published. The validation of the article in question and its importance to researchers and readers must always underwrite such decisions. The editors evaluate articles only for their intellectual content. The editor is guided by the policies of the Journal editorial board and constrained by such legal requirements as shall then be in force regarding issues such as libel, copyright infringement and plagiarism. The editor may confer with other editors or reviewers (or society officers) in making these decisions.

All articles are subjected to Similarity Check. This is an academic plagiarism screening tool, built using a database of current and archival scholarly literature. Similarity Check is a service for editors who want an extra check. The service helps our members to actively engage in efforts to prevent scholarly and professional plagiarism by providing their editorial teams with access to Turnitin's powerful text comparison tool, iThenticate. As Similarity Check members contribute their own published content into iThenticate's database of full-text literature, the service is open to any Crossref member who is actively publishing DOI-assigned article content.

The review process is fair, unbiased, and timely. The papers are reviewed by two independent reviewers. The Journal uses the double-blind review process. If the selected reviewer does not accept the proposal to making a review, the Editorial Board of SJ of PNA may select another reviewer. In cases of controversy additional reviewers are selected. Assessments of all reviewers are treated with due respect. The review is in the written form and concludes with an unequivocal recommendation to accept the article for publication or to reject it.

The editor protects the confidentiality of all material submitted to the journal and all communications with reviewers. The reviewers are not allowed to use their knowledge concerned with the paper prior to its publication. The author is notified of the result of the review process and is provided access to the review once the reviewer's identity has been blinded. Afterwards correspondence with the Editorial Board of SJ of PNA concerned with eventual comments becomes possible.

The list of reviewers cooperating with the Journal is announced once a year.

The Editorial Board of SJ of PNA counteracts against the phenomena of 'ghostwriting' and 'guest authorship'. The editorial team have implemented the procedures described below to exclude unethical practice in publishing research results. Should authors fail to observe them, their paper will not be published. Any signs of lack of integrity and unethical practice will be documented.

Upon acceptance for publication in 'Scientific Journal of Polish Naval Academy' authors are obliged to mail the editors a statement about the authors' contribution to the publication.

The statement must also contain information about the author with the greatest contribution to writing the paper (the main author) and indicate the contribution percentage of other authors in the whole work.

Participation consisting only of raising funds, collecting data (except for papers based only on a survey), or supervising a group of researchers does not justify authorship.

In order to care for the transparency of funding the above mentioned questionnaire also contains the question concerning the source of financing the research.

Authors of the publication must also give information whether the article was presented at the conference or whether it is part of the book being prepared.

Instruction for Authors

All articles should be in the Microsoft Word processor (.doc or .docx). They should not be longer than one author's sheet. Editors may refuse to publish the article.

All articles are subjected to Similarity Check. This is an academic plagiarism screening tool, built using a database of current and archival scholarly literature. For more information about Similarity Check please visit: <https://www.Crossref.org/services/similarity-check/>.

All articles are reviewed. The reviewing procedure complies with the recommendations by the Ministry of Science and Higher Education. Editors (knowledgeable and qualified in the field of study) make initial assessment if papers submitted to the editor's office are suitable for the journal and if review is warranted. Then the papers are reviewed by two independent reviewers. They hold the title of professor or a post-doctoral degree in the specific field and they have the reputation of fair and unbiased reviewers. The Journal uses the double-blind review process. The author is notified of the result of the review process and is provided access to the review once the reviewer's identity has been blinded. Afterwards correspondence with the Editorial Board of SJ of PNA concerned with eventual comments becomes possible.

This journal provides immediate open access to its content under the Creative Commons by 4.0 license. Authors who publish with this journal retain all copyrights and agree to the terms of the above-mentioned [CC BY 4.0 license](https://creativecommons.org/licenses/by/4.0/). Authors are also required to attach to the agreement a statement about the authors' contribution to the publication.

Paper layout:

- title
- first name and last name (surname)
- detailed affiliation
- abstract
- key words
- introduction
- main body including research methodology and obtained results
- conclusions (or summary)
- list of references
- title, abstract and key words in the Polish language

Figures:

- numbered
- signed

Tables:

- numbered
- titled

Formulas:

- numbered
- written in a formula editor

List of references:

- in the alphabetical order
- written in ISO 690 format